Recommendations for Quantification Methods During the Performance of a Pediatric Echocardiogram: A Report From the Pediatric Measurements Writing Group of the American Society of Echocardiography Pediatric and Congenital Heart Disease Council

Leo Lopez, MD, FASE, Chair, Steven D. Colan, MD, FASE, Peter C. Frommelt, MD, FASE, Gregory J. Ensing, MD, FASE, Kathleen Kendall, RDCS, FASE, Adel K. Younoszai, MD, FASE, Wyman W. Lai, MD, MPH, FASE, and Tal Geva, MD, FASE, *Bronx and New York, New York; Boston, Massachusetts; Milwaukee, Wisconsin; Ann Arbor, Michigan; Houston, Texas; Denver, Colorado*

Accreditation Statement:
The American Society of Echocardiography is accredited by the Accreditation Council for Continuing Medical Education to provide continuing medical education for physicians.

The American Society of Echocardiography designates this educational activity for a maximum of 1.5 *AMA PRA Category 1 Credits*™. Physicians should only claim credit commensurate with the extent of their participation in the activity.

ARDMS and CCI recognize the ASE's certificates and have agreed to honor the credit hours toward their registry requirements for sonographers.

The American Society of Echocardiography is committed to ensuring that its educational mission and all sponsored educational programs are not influenced by the special interests of any corporation or individual, and its mandate is to retain only those authors whose financial interests can be effectively resolved to maintain the goals and educational integrity of the activity. Although a monetary or professional affiliation with a corporation does not necessarily influence an author's presentation, the Essential Areas and policies of the ACCME require that any relationships that could possibly conflict with the educational value of the activity be resolved prior to publication and disclosed to the audience. Disclosures of faculty and commercial support relationships, if any, have been indicated.

Target Audience:
This activity is designed for all cardiovascular physicians and cardiac sonographers with a primary interest and knowledge base in the field of echocardiography; in addition, residents, researchers, clinicians, intensivists, and other medical professionals with a specific interest in cardiac ultrasound will find this activity beneficial.

Objectives:
Upon completing the reading of this article, participants will better be able to:

1. Review the techniques for optimizing imaging and quantifying cardiac structures in the pediatric population.
2. Explain the importance of adjusting measurements of cardiovascular structures for the effects of body size.
3. Identify the pediatric quantification protocols for the pulmonary veins, systemic veins, atria and atrioventricular valves.
4. Recognize and apply the recommended echocardiographic methods for the evaluation of left and right ventricular size and systolic function.
5. Define the optimal views and the appropriate anatomic sites for correct measurement of the proximal ascending, proximal and distal arch, and descending aorta.
6. Employ appropriate transducer position and Doppler technique for the anatomic and hemodynamic interrogation of the aorta and aortic valve and the pulmonary artery and the pulmonary valve.

From the Children's Hospital at Montefiore, Bronx, New York (L.L.); Children's Hospital Boston/Harvard Medical School, Boston, Massachusetts (S.D.C., T.G.); Medical College of Wisconsin, Milwaukee, Wisconsin (P.C.F.); the University of Michigan, Ann Arbor, Michigan (G.J.E.); Texas Children's Hospital, Houston, Texas (K.K.); Children's Hospital/University of Colorado, Denver, Colorado (A.K.Y.); and Stanley Morgan Children's Hospital of New York Presbyterian, New York, New York (W.W.L.).

TABLE OF CONTENTS

INTRODUCTION

Echocardiographic quantification is crucial in the diagnosis and management of patients with acquired and congenital heart disease (CHD). The American Society of Echocardiography (ASE) and the European Association of Echocardiography have published recommendations on how to measure the size and function of cardiovascular structures in adults, providing reference limits to distinguish normal from abnormal values.[1] Identifying an abnormal measurement helps assess the effect of a disease on the size of a cardiovascular structure, determine when intervention may be necessary, and monitor the effect of the intervention. Examples in which these standards are useful include aortic root dilation in Marfan syndrome[2-5] and left ventricular (LV) dilation with a ventricular septal defect.[6] However, the size of cardiovascular structures is influenced not only by the hemodynamics of disease states and their treatments but also by confounding factors. such as growth, age, genes, gender, race, body composition, basal metabolic rate, hematocrit, exercise, and altitude.

Aside from abnormal hemodynamics, body size is the most powerful determinant of the size of cardiovascular structures: all cardiovascular structures increase in size relative to somatic growth, a phenomenon known as cardiovascular allometry.[7-10] Expressing measurements relative to body size allows a meaningful distinction between normal and abnormal values in children. It does require the collection of quantitative data from a normal pediatric population to function as the standard against which all measurements are compared. Because there must be agreement on how to measure the size of each cardiovascular structure, this document describes the recommended protocols for the morphometric evaluation of the heart in children with or without CHD, and recommendations at the end of each section refer to measurements that may be useful for the creation of a pediatric normative database. **However, the Pediatric Measurements Writing Group emphasizes that the recommended measurements are those that *can* be** performed in a pediatric examination and not necessarily those that *must* be part of the study.

OPTIMIZATION TECHNIQUES IN IMAGING AND DOPPLER EVALUATION

Standard views are often categorized as "long axis" or "short axis",[11] and these are described in Table 1. General optimization techniques in two-dimensional (2D) imaging have been outlined previously for children.[11] Several technical factors can influence the accuracy of spatial measurements: (1) axial resolution parallel to the ultrasound beam is superior to lateral resolution perpendicular to the beam, so views allowing for linear axial measurements are better than those for which only lateral measurements are available (parasternal views are better than apical views for the aortic annulus); (2) lateral resolution degrades with increasing distance secondary to beam spread, so the transducer should be positioned as close as possible to a structure when only a lateral measurement is available; and (3) for large image depths, the ultrasound resolution often exceeds the pixel resolution of the image display, so decreasing the image depth or magnifying the region of interest can often alleviate the limitations of the monitor resolution.

Quantitative assessment of each structure should be performed in multiple views, and orthogonal planes should be used for noncircular structures such as the atrioventricular (AV) valves. Early reports based on M-mode echocardiography recommended measurements from the leading edge of the near-field reflector to the leading edge of the far-field reflector,[12] and normative data for the proximal aorta in adults have involved leading edge–to–leading edge measurements.[13] However, current guidelines for chamber, annular, and vessel quantification involve measurements of intraluminal dimensions from one inner edge to the opposite inner edge.[14] In addition, published pediatric normative databases based on 2D echocardiography have used inner edge–to–inner edge measurements of vessel diameters.[15-17] There are two important caveats with these measurements: vascular diameters should be perpendicular to the long axis of the vessel, and valvar and vascular diameters should be measured at the moment of maximum expansion. In other words, the inferior vena cava (IVC) diameter should be measured during exhalation, the mitral valve (MV) and tricuspid valve (TV) annular diameters in diastole, and the aortic valve (AoV) and pulmonary valve (PV) annular diameters as well as arterial diameters in systole. These recommendations are based on hemodynamic considerations, correspond to the methodologies used in published pediatric normative databases,[15-17] and often differ from the quantification approach used in adults.[1,13]

General optimization techniques in Doppler echocardiography have been outlined previously for adults,[18] and their utility must address the abnormal valve and vessel positions and unusual flow jets in patients with CHD. Color mapping should precede spectral Doppler interrogation to identify the direction of flow. The audio feature can help optimize alignment, especially given the unpredictable orientation of flow jets in the third dimension. Doppler waveforms should be displayed at a sweep speed of 100 to 150 mm/s to discriminate temporal changes in the velocity flow profile, particularly in children with high heart rates. Simultaneous electrocardiographic display helps correlate the timing of flow with electrical events. Doppler gain and power settings should be optimized to depict the outer edge of the brightest spectral Doppler envelope; only well-defined envelopes should be measured, and "fuzz" or "feathering" beyond modal velocities should be excluded. Mean gradients calculated from the velocity-time integral (VTI) or area under the

Abbreviations
A area = Area under mitral inflow Doppler curve during atrial contraction
A wave = Mitral inflow Doppler component during atrial contraction
a′ wave = Annular tissue Doppler component during atrial contraction
Ar wave = Systemic/pulmonary venous flow reversal during atrial contraction
AoV = Aortic valve
ASE = American Society of Echocardiography
AV = Atrioventricular
BSA = Body surface area
CHD = Congenital heart disease
D wave = Systemic/pulmonary venous Doppler component during diastole
dP/dt = First derivative of pressure with respect to time
E area = Area under mitral inflow Doppler curve during early diastole
E wave = Mitral inflow Doppler component during early diastole
e′ wave = Annular tissue Doppler component during early diastole
EF = Ejection fraction
IVC = Inferior vena cava
IVCT′ = Isovolumic contraction time from tissue Doppler evaluation
IVRT = Isovolumic relaxation time from blood flow Doppler evaluation
IVRT′ = Isovolumic relaxation time from tissue Doppler evaluation
L = Left ventricular length
LA = Left atrial
LV = Left ventricular
MRI = Magnetic resonance imaging
MV = Mitral valve
PFR$_{SV}$ = Peak filling rate/stroke volume
PV = Pulmonary valve
RA = Right atrial
RV = Right ventricular
s′ wave = Annular tissue Doppler component during systole
S wave = Systemic/pulmonary venous Doppler component during systole
SF = Shortening fraction
TAPSE = Tricuspid annular plane systolic excursion
3D = Three-dimensional
TV = Tricuspid valve
2D = Two-dimensional
V = Ventricular volume
VTI = Velocity-time integral

velocity curve should be measured from valve opening to closure at the AV and semilunar valves and throughout the cardiac cycle within a blood vessel or at an interatrial communication, incorporating the zero velocity during periods of absent flow. All Doppler measurements should be averaged over 3 consecutive cardiac cycles to account for respiratory variation.

PRINCIPLES AND METHODS FOR ADJUSTING MEASUREMENTS OF CARDIOVASCULAR STRUCTURES FOR THE EFFECTS OF BODY SIZE

The first step in adjusting for body size involves developing a mathematical description of the mean behavior of the measurement within a normal pediatric population. Ideally, this is based on physiologic principles. Body surface area (BSA) appears to be a better parameter of somatic growth in normal children than height or weight alone.[15,19] Published equations to calculate BSA often produce variable results, particularly at lower height and weight values,[20-23] and some are derived from data that do not include children.[20] The Haycock formula[21] (BSA $[m^2]$ = 0.024265 × weight $[kg]^{0.5378}$ × height $[cm]^{0.3964}$) appears to provide the best correlation between BSA and the size of cardiovascular structures (compared with the formulas of DuBois and DuBois,[20] Dreyer and Ray,[22] and Boyd[23]) and is recommended for calculating BSA.[15] Because of the linear relationship between cardiac output and BSA[24] and the mostly linear relationship between cardiac output and the size of cardiovascular structures,[15] "indexing" the size of structures to BSA has become a fairly common practice.[25-28] However, assuming that BSA is linearly related to length, area, and volume measurements is mathematically impossible. In addition, BSA-adjusted measurements often manifest a persistent dependence on BSA: the mean value of the BSA-adjusted measurement and the distribution of values around the mean change with increasing BSA (a phenomenon of changing or nonconstant variance known as heteroscedasticity).[10,29]

Once the mathematical relationship between a measurement and BSA has been determined, the next step involves the confidence intervals and the problem of heteroscedasticity. One approach to find a mathematical descriptor that maintains a stable and constant variance across the range of body sizes might involve transformation of the measurements and/or BSA within a linear or nonlinear regression equation.[15,17,19] For example, physiologic principles suggest that distances can be adjusted or normalized to the square root of BSA, areas to BSA, and volumes to BSA$^{1.5}$.[30] This approach results in a mostly linear relationship between the measurement and the transformed BSA,[15] but it does not eliminate the problem of heteroscedasticity; variance continues to be affected by changes in body size. Another example involves performing a logarithmic transformation of the measurements to minimize the problem of heteroscedasticity.[17] However, this method does not effectively describe the population at minimum and maximum BSA values, nor does it fully eliminate heteroscedasticity. There is also no fundamental physiologic explanation for this approach.

An increasingly popular approach in pediatric cardiology to account for the effects of body size and age has been the use of Z scores.[15-17,31-36] Calculation of Z scores involves assessment of the distribution of measurement values (by determining the confidence intervals) across a range of body sizes in the normal population. The Z score of a measurement is the number of standard deviations of that value from the mean value at a particular BSA. In other words, a Z score of zero corresponds to a measurement equal to the population mean for that particular BSA. A Z score of +2 or −2 corresponds to

Table 1 Standard echocardiographic views

Recommended terminology	Axis designation	Alternate terminology
Subxiphoid long-axis	Long axis of left ventricle	Subcostal long-axis Subcostal transverse
Subxiphoid short-axis	Short axis of left ventricle	Subcostal short-axis Subcostal sagittal
Apical 4-chamber	Long axis of LV outflow tract	
Apical 3-chamber	Long axis of LV outflow tract	Apical long-axis
Apical 2-chamber	Long axis of LV outflow tract	
Parasternal long-axis	Long axis of LV outflow tract	Left parasternal long-axis
Parasternal short-axis	Short axis of left ventricle	Left parasternal short-axis
High left parasternal	Long axis of MPA-LPA continuation	High left parasagittal Ductal
Suprasternal long-axis	Long axis of ascending and proximal descending Ao displaying aortic arch	Suprasternal aortic arch Suprasternal sagittal
Suprasternal short-axis	Short axis of ascending Ao	Suprasternal transverse
Right parasternal	Long axis of SVC and IVC	High right parasternal Right sternal border Right sternal border long-axis Right sternal border sagittal

Ao, Aorta; *IVC*, inferior vena cava; *LA*, left atrium; *LPA*, left pulmonary artery; *LV*, left ventricle; *MPA*, main pulmonary artery; *SVC*, superior vena cava.

a measurement that is 2 standard deviations above or below the mean for that particular BSA, thresholds that usually represent the upper or lower limits of normal. Z scores can be converted to percentiles, though the magnitude of an abnormality is much easier to appreciate with Z scores than with percentiles (for example, a Z score of +4 corresponds to the 99.8th percentile, and Z score of +10 corresponds to the 99.9th percentile). The major advantage of using Z scores has been the absence of any reliance on a predetermined relationship between the size of a structure and BSA. In addition, there is no assumption that a constant variance exists across the range of body sizes within the pediatric population. However, the utility of some published Z-score approaches has been limited by the fact that a "normal" population is frequently identified as those individuals with normal results on echocardiography, a truly self-referential definition. Second, the approach does not always account for such confounders as gender and race. Last, the methodologies for performing measurements and calculating BSA are often inconsistent across the entire population being evaluated.

Recommendations: When normative data are available, the measurements of cardiovascular structures should be expressed as Z scores using the Haycock formula[21] to calculate BSA.

PEDIATRIC QUANTIFICATION PROTOCOLS

Pulmonary Veins, Systemic Veins, and Atria

Morphometric Evaluation. The pulmonary veins are usually best evaluated in a high left parasternal or suprasternal short-axis view ("crab" view) displaying drainage of the right and left pulmonary veins into the left atrium. Dual display without and with low-scale color mapping helps identify the individual pulmonary veins, and the diameter of each pulmonary vein before it connects to the left atrium can be measured from the 2D image. The left atrial (LA) appendage should not be mistakenly identified as the left upper pulmonary vein, and the right middle pulmonary vein should not be

mistakenly identified as the right upper pulmonary vein (subxiphoid short-axis or right parasternal views are usually better at displaying the right upper pulmonary vein). The superior vena cava is not routinely measured in clinical practice, and normative data have not been established. IVC size can be measured above its junction with the hepatic veins just below the diaphragm in subxiphoid short-axis views (displaying the IVC long axis), and this may help assess hydration status.[37,38] The IVC diameter varies with respiration, and the collapsibility index (the percentage decrease in IVC diameter with inspiration) appears to correlate with right atrial (RA) pressures in adults.[1,39,40] Neither the IVC diameter nor the collapsibility index, however, appears to correlate with age or BSA in adult patients,[39] and the utility of the collapsibility index in children has not been evaluated.

LA size can be assessed by M-mode and 2D measurements of the distance from the posterior aortic wall to the posterior LA wall,[41] though this anteroposterior distance correlates poorly with angiographically derived LA volumes.[42] Recent recommendations involve the calculation of LA volumes from apical views at end-systole just before the MV opens using major-axis and minor-axis dimensions and planimetered areas in orthogonal views (Figure 1). As with all measurements performed in apical views, care must be taken not to foreshorten the heart. Among all LA volume calculations, the biplane area-length and the biplane Simpson (summation of disks) methods using apical 4-chamber and 2-chamber views appear to provide the most consistent results with published reference values for normal adults.[1,43,44] The biplane area-length method has also been used in children, and LA volumes indexed to BSA appear to correlate with diastolic function and mitral regurgitation grade.[45] Last, LA volumes have been calculated using real-time three-dimensional (3D) echocardiography and a rotation/polyhedral surface algorithm, and these have correlated well with LA volumes measured by magnetic resonance imaging (MRI).[46]

RA size is usually assessed in an apical 4-chamber view at end-systole just before the TV opens (Figure 2).[1,43,47-50] Major-axis and minor-axis dimensions are significantly different between normal adults and
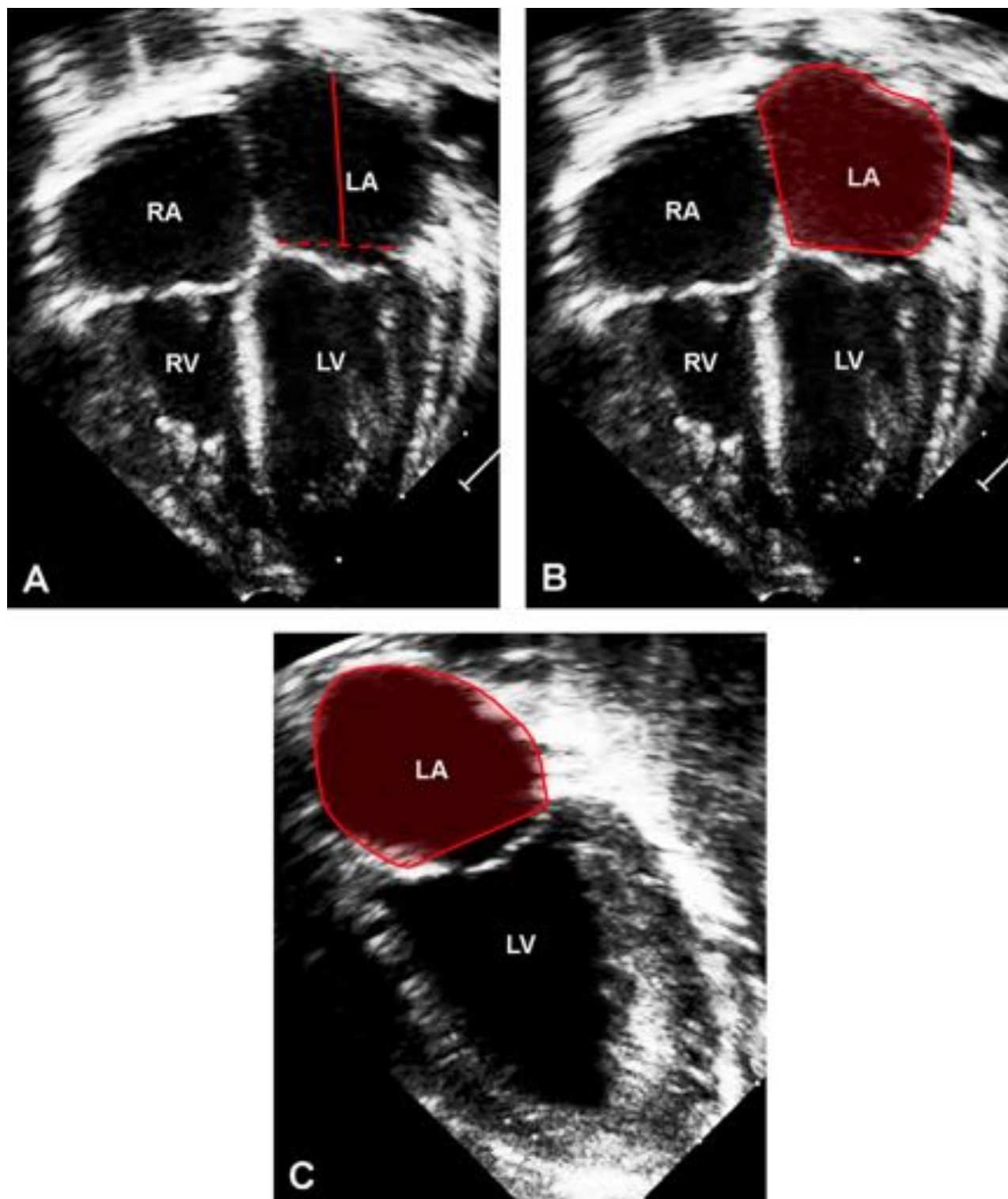
Figure 1 Apical 4-chamber and 2-chamber views at ventricular end-systole showing **(A)** left atrial major-axis length in a 4-chamber view, **(B)** left atrial planimetered area in a 4-chamber view, and **(C)** left atrial planimetered area in a 2-chamber view. *LA*, Left atrium; *LV*, left ventricle; *RA*, right atrium; *RV*, right ventricle.

patients with right ventricular (RV) volume overload (from an atrial septal defect or tricuspid regurgitation).[47] Raw values and indexed values on the basis of BSA in normal adults are available.[1,48] Planimetered RA areas or RA volumes calculated from the product of RA area and major-axis length may be better at assessing RA size, though the sample

sizes in most studies have been small.[43,49,50] As with LA volumes, 3D echocardiography may provide a useful means by which to measure RA volumes using the polyhedral surface algorithm.[46,50]

Recommendations (Table 2): The recommended methods to assess LA size include the measurement of
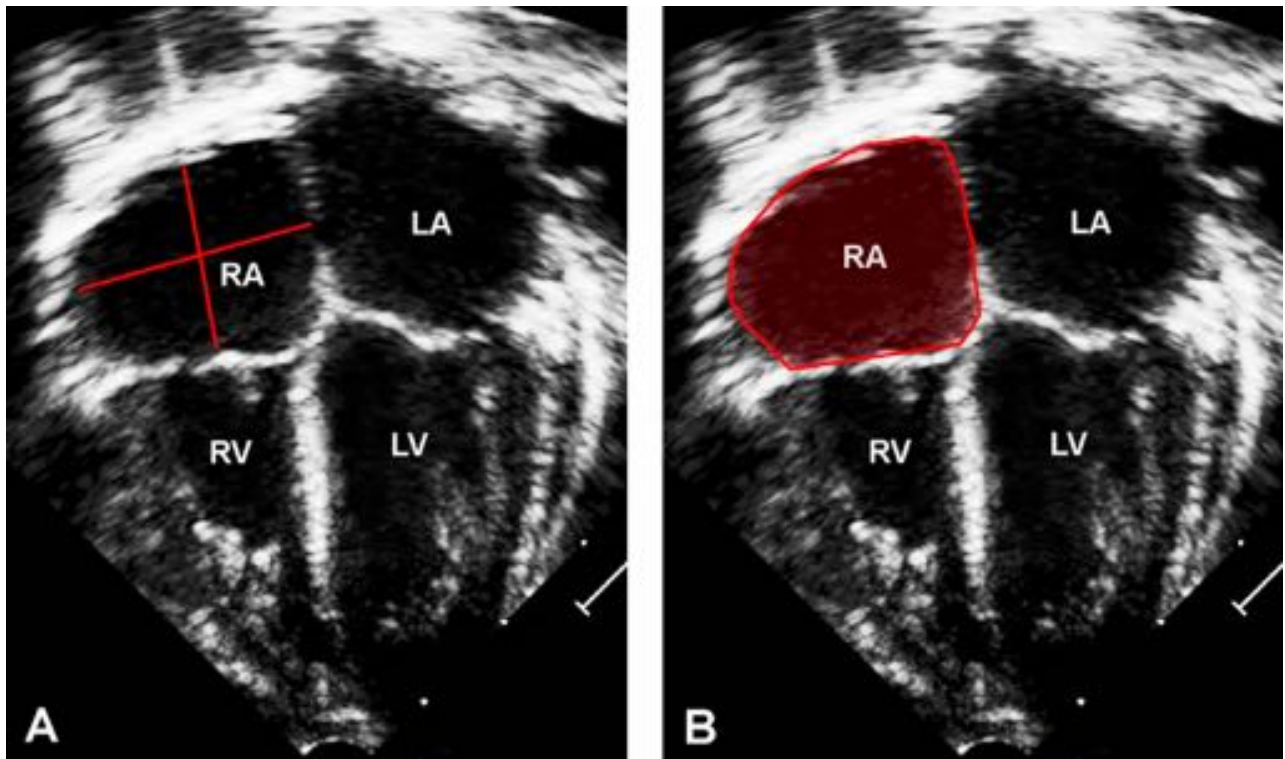
Figure 2 Apical 4-chamber view at ventricular end-systole showing **(A)** right atrial major-axis and minor-axis lengths and **(B)** right atrial planimetered area. *LA*, Left atrium; *LV*, left ventricle; *RA*, right atrium; *RV*, right ventricle.

major-axis lengths in apical 4-chamber views and planimetered areas in orthogonal apical views and calculation of volumes using the biplane area-length or the biplane Simpson method. The recommended methods to assess RA size include the measurement of major-axis and minor-axis lengths and planimetered areas in apical 4-chamber views. When the IVC diameter is measured, measurement should be performed above its junction with the hepatic veins just below the diaphragm in subxiphoid short-axis views.

Doppler Evaluation. Pulsed-wave Doppler interrogation of pulmonary and systemic venous flow requires precise placement of the sample volume in the lumen of the vessel >5 mm from its ostium. Because venous flow velocities are low, the Doppler high-pass filter should be minimized. Pulmonary venous flow is usually evaluated in apical or parasternal views, whereas superior vena cava flow can be evaluated in subxiphoid or suprasternal views. IVC flow is best evaluated in subxiphoid views; hepatic vein flow is usually used as a surrogate because the hepatic veins are more parallel to the line of interrogation than the IVC.[51,52] Characterization of pulmonary and systemic venous Doppler patterns can help with the assessment of atrial and ventricular diastolic function as well as AV valve function (Figure 3).[53] Antegrade flow during ventricular systole (S wave) occurs because of both atrial relaxation and apically directed movement of the AV annulus.[54] Occasionally, it is biphasic secondary to temporal dissociation of the two components. Abnormal retrograde flow during ventricular systole can occur in the setting of significant AV valve regurgitation[55] as well as AV electrical dissociation with atrial contraction against a closed AV valve during ventricular systole.[56] Antegrade flow during ventricular diastole (D wave) is influenced by atrial and ventricular filling properties

as well as AV valve patency. With fast heart rates, the S and D peaks may fuse.[54] Retrograde flow during atrial contraction (Ar wave) is frequently augmented when ventricular compliance is decreased.[54] In fact, a pulmonary vein Ar wave duration that exceeds the MV inflow duration during atrial systole predicts increased LA and LV end-diastolic pressures in the setting of reduced ventricular compliance.[57,58] Both the systemic venous D and Ar waves can be affected by respiration, with increased D-wave and decreased Ar-wave velocities during inspiration secondary to negative intrathoracic pressure, so these measurements should be averaged over 3 consecutive cycles.[59,60]

Recommendations (Table 2): Pulmonary venous S-wave, D-wave, and Ar-wave velocities and Ar-wave duration are best measured in apical or parasternal short-axis views.

AV Valves

Morphometric Evaluation. Measurement of MV and TV size helps characterize valvar pathology and diagnose ventricular hypoplasia.[61-64] Annular diameter and area can be measured by 2D and 3D imaging.[65-70] Annular area may also be estimated from a single-plane diameter using the area formula for a circle,[69,71] but the MV annulus is in fact elliptical and saddle-like in shape.[70,72] A more accurate estimate can be obtained with orthogonal diameters using the area formula for an ellipse ($[\pi/4 \times \text{diameter}_1 \times \text{diameter}_2]$). Echocardiographic measurements of MV size generally overestimate postmortem measurements,[65,73] but this may be an artifact of tissue fixation. Published pediatric normative databases have used annular diameters measured in apical 4-chamber (lateral diameter) and parasternal long-axis (anteroposterior diameter) views to calculate MV and TV elliptical annular areas (Figure 4).[15] However, recent studies in adult patients suggest that apical 2-chamber and 3-chamber

Table 2 Measurements of the Pulmonary Veins, Systemic Veins, and Atria

Measurement	View	Timing/Location	Applications	Strengths	Weaknesses
LA major-axis length	Apical 4-chamber	Ventricular end-systole*	LA size	Better than M-mode or 2D antero-posterior length Normal adult data[1] Some normal pediatric data[17]	Foreshortening Little normal pediatric data
LA minor-axis length	Apical 4-chamber	Ventricular end-systole*	LA size	Same as above	Same as above
LA planimetered area$_{4C}$	Apical 4-chamber	Ventricular end-systole*	LA size	Same as above	Same as above
LA planimetered area$_{2C}$	Apical 2-chamber	Ventricular end-systole*	LA size	Same as above	Same as above
RA major-axis length	Apical 4-chamber	Ventricular end-systole*	RA size	Normal adult data[1]	Same as above
RA minor-axis length	Apical 4-chamber	Ventricular end-systole*	RA size	Normal adult data[1]	Same as above
RA planimetered area	Apical 4-chamber	Ventricular end-systole*	RA size	Better than 2D length	Same as above
IVC diameter	Subxiphoid short-axis	Just below diaphragm	Hydration status RA pressure	Respiratory variation	No normal pediatric data
Pulmonary vein S velocity	Apical or parasternal short-axis	Systole	LV diastolic function LA function MV function		Depends on alignment
Pulmonary vein D velocity	Apical or parasternal short	Diastole	Same as above		Depends on alignment
Pulmonary vein Ar velocity	Apical or parasternal short	Diastole	Same as above		Depends on alignment
Pulmonary vein Ar duration	Apical or parasternal short	Diastole	Same as above		Depends on alignment

Calculation	View	Formula	Applications	Strengths	Weaknesses
LA volume	Apical	Area-length: $\frac{8 \times A_{4C} \times A_{2C}}{3 \times \pi \times h}$	LA size	Normal adult data[1]	Foreshortening No normal pediatric data
LA volume	Apical	Summation of disks: $\frac{\pi}{4} \times \sum_{i=1}^{N} ai \times bi \times \frac{h}{N}$	LA size	Normal adult data[1]	Foreshortening No normal pediatric data

4C, 4-chamber; *2C,* 2-chamber; a_i, minor-axis slice radius in apical 4-chamber view; A_{4C}, area in the apical 4-chamber view; A_{2C}, area in the apical 2-chamber view; b_i, minor axis slice radius in apical 2-chamber view; *h*, shortest LA major-axis length in either apical 4-chamber view or 2-chamber view; *IVC*, inferior vena cava; *LA*, left atrial; *MV*, mitral valve; *N*, number of slices; *RA*, right atrial.
*One frame before MV or TV opening.
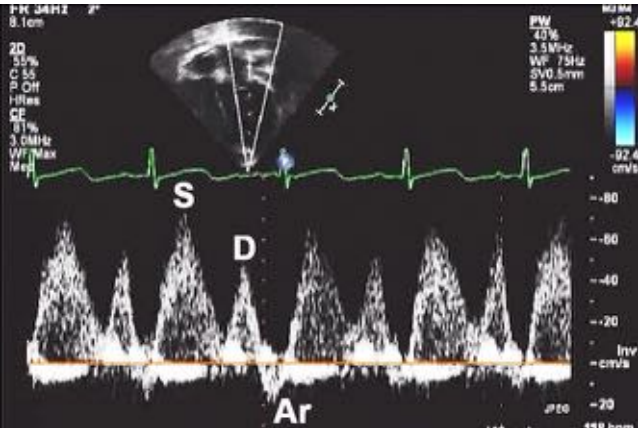
Figure 3 Pulmonary vein Doppler pattern. *Ar*, Peak retrograde flow velocity during atrial contraction; *D*, peak antegrade flow velocity during ventricular diastole; *S*, peak antegrade flow velocity during ventricular systole.

views of the MV provide better anatomic alignment and more accurate MV annular dimensions compared with measurements obtained by computed tomography.[74] The difficulty of obtaining adequate 2-chamber views in children often precludes the use of this technique, and most pediatric studies involving various CHDs are based on MV and TV annular measurements obtained in apical 4-chamber and parasternal long-axis views.

The largest diameters during peak filling in early diastole should be measured at the frame after maximum excursion of the leaflets from inner edge to inner edge at the hinge points of the leaflet attachments.[18] Nomograms for MV and TV diameters are available.[15,16,30,31,75] Although 2D planimetry has been demonstrated to be reasonably accurate in adults with acquired MV stenosis,[76] it is unreliable in the setting of congenital MV stenosis, which is characterized by complex multilevel obstruction with abnormally shaped and often multiple flow orifices precluding a true single-plane "en face" view of the maximum orifice area. Compared with 3D planimetric assessment in patients with mitral stenosis, 2D planimetry overestimates MV area by as much as 88%, depending on valve geometry (domed vs funnel shape) and the position of the transducer relative to the valve orifice.[77]

Recommendations (Table 3): The recommended methods to assess MV and TV annular size include measurement of lateral diameters in apical 4-chamber views and anteroposterior diameters in parasternal long-axis views and calculation of areas using the area formula for an ellipse.
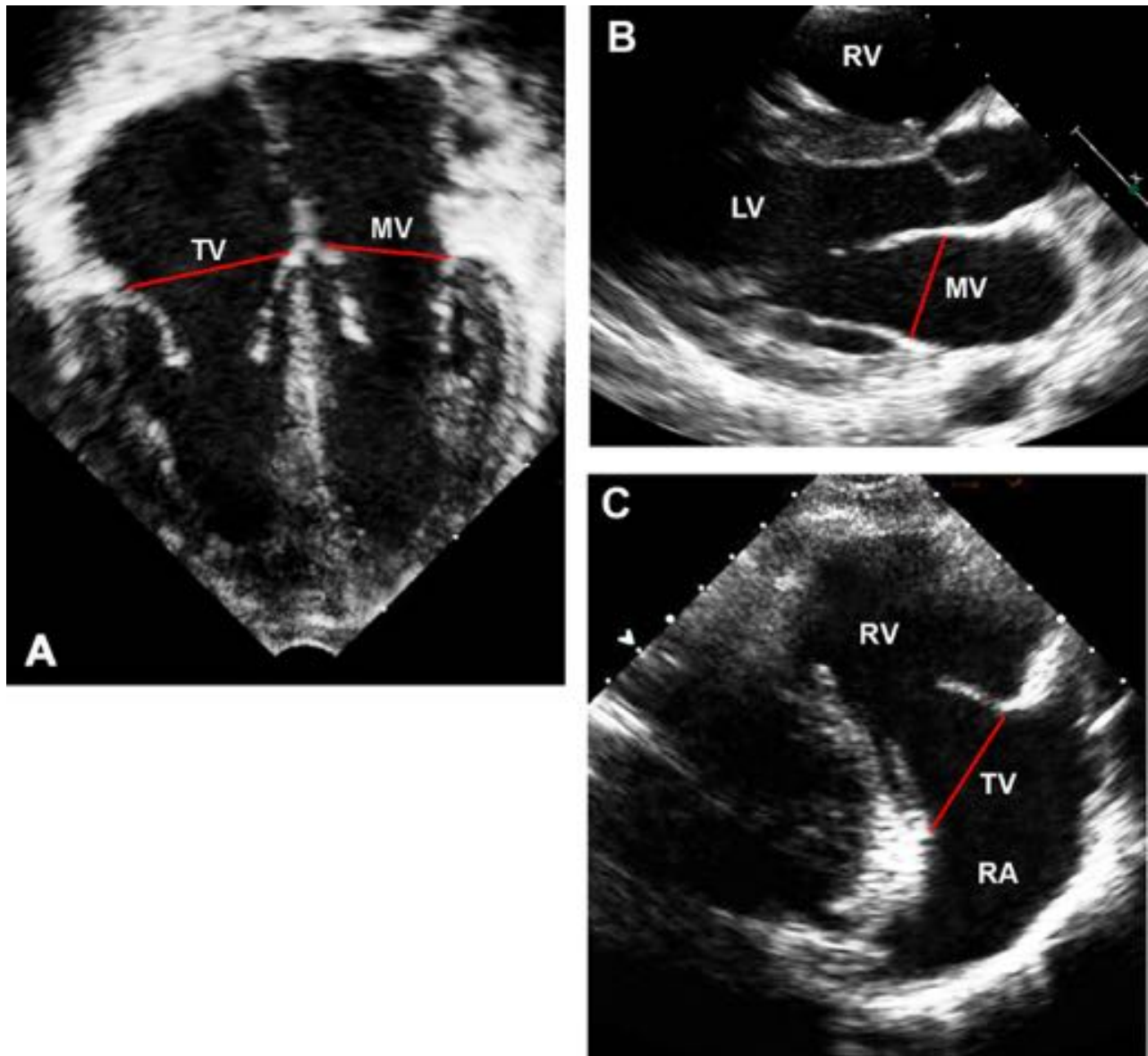
Figure 4 **(A)** Mitral and tricuspid annular diameters in an apical 4-chamber view, **(B)** mitral annular diameter in a parasternal long-axis view, and **(C)** tricuspid annular diameter in a parasternal long-axis view. *LV*, Left ventricle; *RA*, right atrium; *RV*, right ventricle.

Doppler Evaluation. Doppler interrogation of ventricular inflow is best performed with the help of color mapping in apical views where transducer position and angulation changes are frequently needed to optimize alignment. When MV or TV stenosis is suspected, the VTI of the inflow tracing from continuous-wave Doppler interrogation is used to calculate the mean gradient and assess the severity of obstruction. It is important to remember, however, that the transvalvar gradient is dependent on the diastolic filling period and can be augmented by the faster heart rates in children.[78] Stenosis can also be evaluated by measuring the pressure half-time (the time needed for the peak early diastolic pressure to decline by 50%) or calculating the effective orifice area from the continuity equation (the stroke volume or the product of cross-sectional area and the blood flow VTI at that location is preserved at each position along a closed system).[79] However, these methods are also limited by the faster heart rates in children, correlate poorly

with data derived from catheterization in the setting of congenital AV valve stenosis,[80] and are not recommended for routine use in children. Quantitative assessment of MV and TV regurgitation has been discussed previously for adults.[81] Some of the recommended Doppler methods have included measurement of the vena contracta diameter and the regurgitant jet area as well as calculation of the regurgitant volume, regurgitant fraction, and effective regurgitant orifice area from the continuity equation and from the proximal isovelocity surface area phenomenon. However, the utility of these indices in children is limited, and they have not been validated.

Pulsed-wave Doppler analysis of MV inflow velocities is used frequently to assess LV diastolic function.[53,82-84] The sample volume is best positioned in the left ventricle at the tips of the valve leaflets (distal to the annulus) because both the peak early diastolic velocity (E wave) and the peak velocity during atrial contraction (A wave) decrease significantly in value as the sample volume is moved

Table 3 Measurements of the Atrioventricular Valves

Measurement	View	Timing	Applications	Strengths	Weaknesses
Lateral MV diameter (MVD$_L$)	Apical 4-chamber	Diastole*	MV size	Reproducible Normal adult data[72] Normal pediatric data[15-17, 30, 31]	May not be as good as apical 2-chamber and apical 3-chamber measurements[74]
Antero-posterior MV diameter (MVD$_{AP}$)	Parasternal long-axis	Diastole*	MV size	Same as above	Same as above
Lateral TV diameter (TVD$_L$)	Apical 4-chamber	Diastole*	TV size	Same as above	
Antero-posterior TV diameter (TVD$_{AP}$)	Parasternal long-axis	Diastole*	TV size	Same as above	
MV E wave peak velocity	Apical 4-chamber	Diastole	LV diastolic function		Depends on alignment & sample volume location Depends on loading conditions
MV A wave peak velocity	Apical 4	Diastole	LV diastolic function		Same as above
MV A wave duration	Apical 4	Time from beginning to end of A wave	LV diastolic function		Fast heart rates in children → fusion of E and A waves
MV deceleration time	Apical 4	Time from E wave peak velocity to return to baseline	LV diastolic function		Fast heart rates in children → fusion of E and A waves
Isovolumic relaxation time (IVRT)[†]	Apical 3-chamber	Time from AoV closure to MV opening with simultaneous CW Doppler of LV outflow and inflow	LV diastolic function		Fast heart rates in children → poor temporal resolution

Calculation	View	Formula	Applications	Strengths	Weaknesses
MV area	Apical 4-chamber/ parasternal long-axis	$\frac{\pi}{4} \times MVD_L \times MVD_{AP}$	MV size	Reproducible Normal adult data[72] Normal pediatric data[15, 16, 30, 31]	Assumes elliptical shape Measures annular area and not valvar area
TV area	Apical 4-chamber/ parasternal long-axis	$\frac{\pi}{4} \times TVD_L \times TVD_{AP}$	TV size	Same as above	Assumes elliptical shape Measures annular area and not valvar area
E/A ratio	Apical 4-chamber	E wave peak velocity/ A wave peak velocity	LV diastolic function		Fast heart rates in children → fusion of E and A waves

CW, Continuous wave; *MV*, mitral valve; *MVD$_{AP}$*, anteroposterior MV diameter; *MVD$_L$*, lateral MV diameter; *TV*, tricuspid valve; *TVD$_{AP}$*, anteroposterior TV diameter; *TVD$_L$*, lateral TV diameter.
*Maximum diameter.
†Measured by blood flow Doppler evaluation rather than by tissue Doppler evaluation, as described in Table 4.

toward the atrium (Figure 5A).[85] The isovolumic relaxation time (IVRT), representing the time from AoV closure to MV opening, can be measured from the aortic component of the second heart sound using a phonocardiogram to the onset of diastolic flow in the MV Doppler tracing or by using simultaneous continuous-wave Doppler interrogation of LV inflow and outflow in an apical 3-chamber view (Figure 5B). The deceleration time from the peak E-wave ve-

locity to its return to baseline in mid-diastole is another parameter of diastolic function that is sensitive to ventricular relaxation and compliance as well as atrial pressure (Figure 5C). However, deceleration time and other diastolic indices based on the E and A waves are limited by their dependence on loading conditions, and their utility in children is often precluded by fusion of the E and A waves resulting from rapid heart rates.
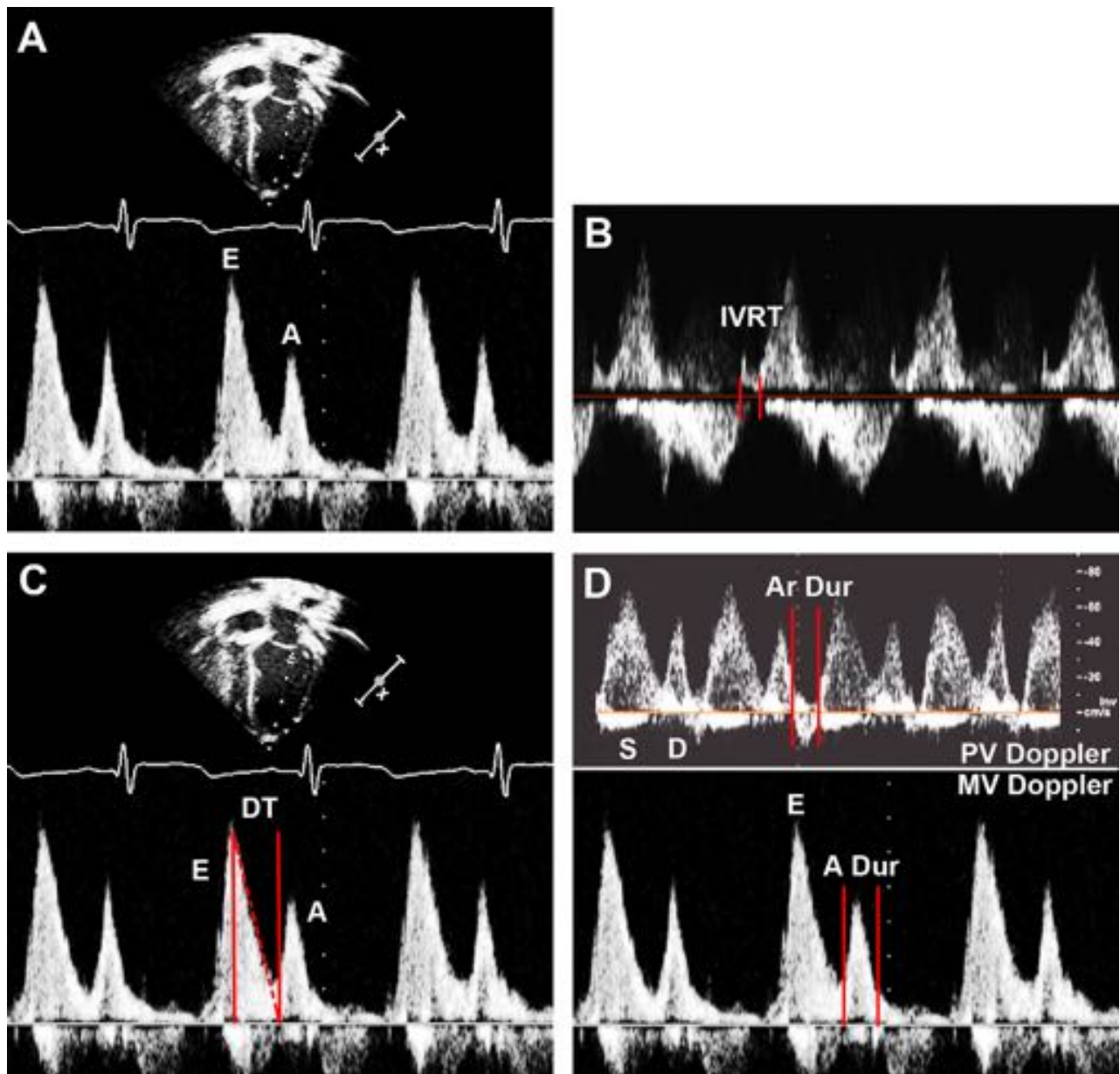
Figure 5 (A) Pulsed-wave Doppler pattern of mitral inflow showing peak velocities during early diastole and atrial contraction, **(B)** continuous-wave Doppler pattern of mitral inflow and LV outflow showing IVRT, **(C)** pulsed-wave Doppler pattern of mitral inflow showing deceleration time (DT), and **(D)** pulsed-wave Doppler patterns of pulmonary venous flow and mitral inflow showing the duration of flow during atrial contraction. *A*, Peak mitral flow velocity during atrial contraction; *A Dur*, time duration of mitral flow during atrial contraction; *Ar Dur*, time duration of retrograde pulmonary venous flow during atrial contraction; *D*, peak antegrade pulmonary venous flow velocity during ventricular diastole; *DT*, deceleration time; *E*, peak mitral flow velocity during early ventricular diastole; *IVRT*, isovolumic relaxation time; *MV*, mitral valve; *PV*, pulmonary vein; *S*, peak antegrade pulmonary venous flow velocity during ventricular systole.

LV diastolic filling can also be characterized by using several calculations[86]: the ratio between the E-wave and A-wave velocities; the E-area and A-area fractions, comparing the VTI during early diastole (E area) and during atrial contraction (A area) with the total area under the diastolic curve; the area or filling fraction in the first 33% (one third filling faction) or the first 50% (one half filling fraction) of diastole; the ratio between pulmonary vein Ar-wave duration and MV A-wave duration as discussed previously[57] (Figure 5D); and peak ventricular filling rates from the product of the E velocity and MV annular cross-sectional area. Because filling rates may vary with cardiac output, it may be more useful to calculate peak filling rates normalized to stroke volume (PFR$_{SV}$) using the following equation[87]:

$$PFR_{sv}(s^{-1}) = peak\ E\ velocity\ (cm/s)/MV\ VTI\ (cm).$$

However, an important limitation with this approach involves the fact that calculations of LV inflow (flow across the MV annulus) and peak filling rates using pulsed-wave Doppler interrogation do not account for MV annular displacement away from the transducer during

diastole; hence, the Doppler profiles used in these calculations actually represent flow toward the transducer rather than true flow across the MV annulus.

Recommendations (Table 3): The recommended methods to assess MV inflow include measurements of E-wave and A-wave velocities, A-wave duration, deceleration time, and IVRT and calculation of the E/A ratio.

Left Ventricle

Morphometric Evaluation. Measurements of LV size and function are essential in the assessment of patients with congenital and acquired heart diseases.[11] Although qualitative visual inspection might be adequate, it can be misleading, is prone to interobserver and interstudy variability, and relies on the skill of the interpreter.[88] Given the impact of quantitative data on diagnosis and management,[89,90] the importance of accurate, reproducible LV measurements cannot be overstated. Although published ASE recommendations for chamber quantification in adults[1] have been used extensively in children, data on the accuracy and reproducibility of these measurements in pediatrics are scant. In addition, there are limitations to the published methods adjusting for body size in adults as discussed previously.[15] Several linear and volumetric methods to assess LV size have been described and integrated into routine clinical practice, each with distinct advantages and weaknesses, and these are discussed in this section.

In general, LV size should be measured during both diastole and systole, defining end-diastole as the frame with the maximum chamber intraluminal area and end-systole as the frame with the minimum area. However, these definitions are problematic because they rely on visual estimates of areas rather than a quantitative frame-by-frame analysis. In addition, the minimum area occurs at different times in short-axis and long-axis views. During isovolumic contraction, the long axis first shortens and then elongates (the reverse process occurs during isovolumic relaxation). In contrast, the short-axis area first increases and then decreases progressively during isovolumic contraction. Given these limitations, end-diastole can be defined as the frame at which the MV closes and end-systole as the frame preceding MV opening.

Short-axis or minor-axis measurements of LV internal diameter and septal and posterior wall thickness can be obtained in parasternal views (Figure 6), though occasionally these measurements are available only in subxiphoid views. The maximum short-axis dimension is often located at the level of the MV leaflet tips or chordae in young patients and more apically at the level of the papillary muscles in older patients and some adults. It is important to note that linear measurements characterize LV size only in one dimension and may misrepresent an abnormally shaped chamber. Short-axis diameters should be considered a surrogate for LV size only when the LV short-axis geometry is circular, a condition often not met in patients with CHD or other abnormal hemodynamic states. Linear measurements can be obtained from long-axis or short-axis views and from M-mode tracings or 2D images. The ASE guidelines for adults recommend linear minor-axis measurements of the left ventricle in parasternal long-axis views because this ensures a perpendicular orientation between the measurement and the LV long axis.[1,85] In addition, limited parasternal windows can overestimate minor-axis diameters with oblique measurements in apically located short-axis views, a problem not seen with long-axis views in nonstandard parasternal locations. However, a long-axis view does not account for the lateral motion of the left ventricle seen in many children and it does not guarantee circular LV short-axis geometry throughout the cardiac cycle. It also forces the use of a single diameter, in contrast to the multiple diameters available
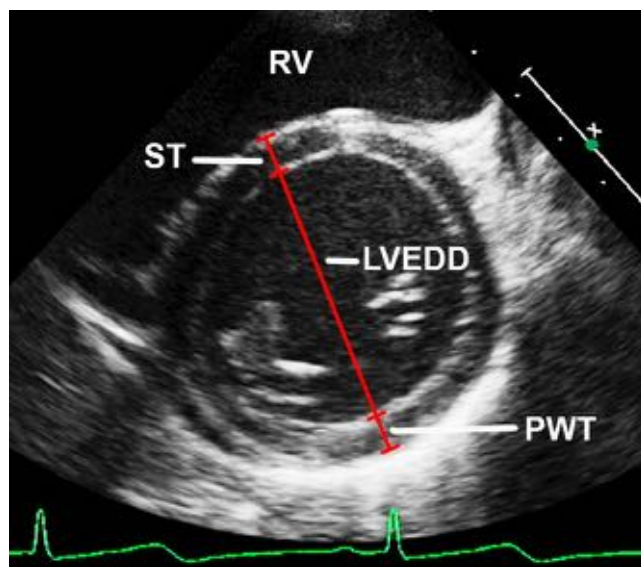
Figure 6 Left ventricular minor-axis (short-axis) measurements of internal diameter (LVEDD), posterior wall thickness (PWT), and septal wall thickness (ST) in a parasternal short-axis view at end-diastole. *RV*, Right ventricle.

from 2D short-axis images. Consequently, the short-axis view is the recommended approach because it allows one to choose the diameter with the best blood-endocardium interface, a definite advantage when dealing with LV trabeculations. In addition, normal pediatric data from M-mode short-axis views are available.[15,91,92]

M-mode echocardiography has provided better temporal and spatial resolution than 2D imaging in the past. However, M-mode measurements in long-axis views can overestimate LV minor-axis diameters compared with 2D measurements.[85] In addition, measurements along a line crossing the midpoints of the ventricular septum and posterior wall (on the basis of the location of the papillary muscle groups) can be difficult by M-mode.[1] Refinements in transducer technology and image processing have recently provided 2D imaging with improved resolution and clear delineation of the blood-endocardium interface. Therefore, 2D short-axis imaging is the recommended approach to obtain LV short-axis measurements averaged over 3 consecutive cardiac cycles (Figure 6). Ideally, a combination of long-axis and short-axis views should be used to ascertain that the short-axis or minor-axis measurement is perpendicular to and crosses the midpoints of the ventricular septum and posterior wall and that the LV short-axis geometry is circular throughout the cardiac cycle.

Two-dimensional volumetric methods require quality LV images from parasternal short-axis, apical, and/or subxiphoid views in which the LV major-axis length and area of the LV endocardial border can be measured. The basal border is defined as the line connecting the MV annular hinge points. The LV length is measured from the basal border midpoint to the apical endocardium, requiring clear images of the apical endocardium without foreshortening the left ventricle. The endocardial border is traced manually, requiring clear delineation of the blood-endocardium interface (convention excludes the papillary muscles when tracing the endocardial border, leaving them included in the blood pool). The biplane Simpson method to calculate LV volumes by summation of equidistant disks is used frequently in adults, with few data validating its accuracy and reproducibility in children. It involves tracing the LV endocardial border in apical 4-chamber and 2-chamber views and using the formula
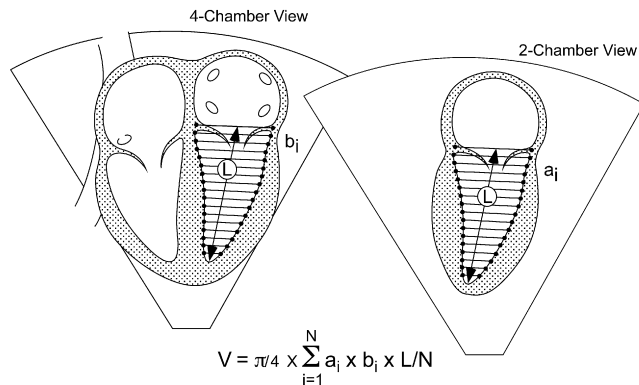
Figure 7 Simpson biplane method for calculating LV volume.

$$V = \frac{\pi}{4} \times \sum_{i=1}^{N} a_i \times b_i \times \frac{L}{N},$$

where V is volume, a_i is the minor-axis slice radius in the apical 4-chamber view, b_i is the minor-axis slice radius in the apical 2-chamber view, L is the LV major-axis length, and N is the number of slices (Figure 7). Some have suggested that the apical 3-chamber view can be substituted for the apical 2-chamber view.[93,94] In children with abnormally shaped left ventricles, the modified Simpson algorithm using a combination of short-axis and long-axis views may be better than the biapical algorithm described above.[95,96] LV volume can also be measured with the area-length or bullet method using the formula $V = 5/6 \times$ short-axis basal area $\times$ LV length (Figure 8).[97] Here, the short-axis basal area is measured from parasternal or subxiphoid short-axis views, and LV length is measured from apical 4-chamber or subxiphoid long-axis views. The truncated ellipse method is similar to the area-length method, with a somewhat different formula requiring the additional measurement of the LV minor-axis diameter from an apical 4-chamber view.

LV mass can be calculated from M-mode or 2D linear measurements,[98-100] and this approach has been used extensively in adult clinical trials and epidemiologic studies.[1,100] It has been used in children,[101-103] though accuracy and reproducibility data, especially in infants, are scant. The most common method is to measure volumes using one of the approaches discussed previously. LV mass is then calculated by subtracting the endocardial volume from the epicardial volume and multiplying this difference (the myocardial volume) by 1.05 g/mL, the myocardial-specific density. LV volume and mass can also be measured using 3D echocardiography, and growing experience suggests that better accuracy can be achieved compared with 2D methods when MRI is used as the gold standard.[104-108] Initial reports in pediatrics are encouraging,[109,110] particularly considering that 3D echocardiography does not rely on geometric assumptions, an important advantage in patients with CHD and abnormally shaped ventricles. However, the feasibility, applicability, and reproducibility of this approach in clinical practice warrant further investigation.

LV systolic function can be evaluated as pump function (global chamber performance) or myocardial function (performance of cardiac myofibers). Global systolic pump function is dependent on myocardial force generation characteristics (contractility) as well as preload, afterload, and heart rate, whereas myocardial function represents myocardial contractility independent of loading conditions and heart rate. Numerous echocardiographic methods have been used to evaluate both properties of LV systolic function, and these can be di-
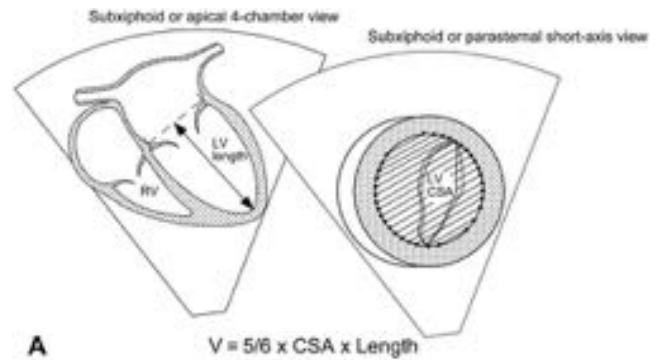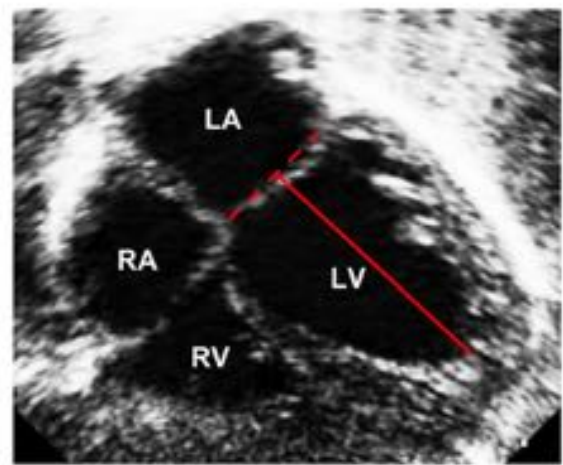
Figure 8 (A) Area-length method for calculating left ventricular volume, (B) left ventricular length in a subxiphoid long-axis view at end-diastole, and (C) left ventricular basal area in a subxiphoid short-axis view at end-diastole. CSA, Cross-sectional area; LA, left atrium; LV, left ventricle; RA, right atrium; RV, right ventricle.

vided into geometric and nongeometric parameters. Geometric parameters require LV dimension or volume measurements and are influenced by LV shape. Nongeometric parameters do not require these measurements, are not affected by LV shape, and rely on Doppler echocardiography and other techniques.

The most commonly used geometric parameters of global LV systolic function are the linear shortening fraction (SF), fractional area change, and the volumetric ejection fraction (EF). These methods are affected by loading conditions, but fractional area change and EF are less sensitive to abnormal chamber geometry and regional

abnormalities. SF can be calculated using LV minor-axis internal diameters obtained from a standard M-mode tracing or from 2D images using the equation SF = (end-diastolic dimension − end-systolic dimension)/end-diastolic dimension. As discussed previously, the 2D approach provides better display of the midpoints of the ventricular septum and posterior wall. EF is calculated from the equation EF = (end-diastolic volume − end-systolic volume)/end-diastolic volume; both end-diastolic and end-systolic volumes are measured using any of the 2D or 3D methods described previously. Extrapolation of EF from linear LV minor-axis diameters is discouraged, because of inaccuracies resulting from geometric assumptions.[1] A relatively load independent index of myocardial function is useful when following patients at risk for abnormal afterload, such as patients undergoing chemotherapy[111] and those infected with human immunodeficiency virus.[112] One such method involves the relationship between velocity of circumferential fiber shortening adjusted for heart rate and end-systolic wall stress, and this index of contractility is relatively independent of preload and incorporates afterload and heart rate in its assessment (Figure 9).[113] However, this index applies only when the LV is normally shaped.

Recommendations (Table 4): The recommended methods to assess LV size and function include a linear approach and a volumetric approach. The linear method involves measurement of short-axis diameters and wall thickness and calculation of SF and the velocity of circumferential fiber shortening adjusted for heart rate and end-systolic wall stress from 2D short-axis images obtained in parasternal or subxiphoid short-axis views. The volumetric method involves (1) measurement of areas from the same 2D or 3D short-axis images; (2) measurement of long-axis lengths from 2D or 3D long-axis images obtained in apical 4-chamber or subxiphoid long-axis views; and (3) calculation of volumes, EF, and mass using 2D or 3D measurements.

Doppler Evaluation. Tissue Doppler evaluation involves pulsed-wave Doppler interrogation of myocardial motion rather than blood flow, and this modality has provided new nongeometric parameters to assess ventricular function.[82-84,114-116] Both AV valves have circumferential annular attachments to the ventricular myocardium, and each annulus is displaced along the longitudinal axis away from the apex in diastole and toward the apex in systole. MV annular motion is assessed at its lateral and septal junctions, whereas TV annular motion is assessed only at its lateral junction (Figure 10). The apical 4-chamber view provides an ideal window for the ventricular longitudinal axis, with little lateral motion ("rocking") of the annulus during the cardiac cycle. Transducer position and angulation should be optimized to maintain Doppler alignment parallel to the direction of maximum annular motion. In children, annular velocities are best measured with a sample volume gate length of <5 mm.[117,118] Because of the low-velocity Doppler signal of the myocardium, the Nyquist limit should be decreased to maximize the deflection size on the display (generally 15-30 cm/s) while using the lowest filter settings. In addition, decreasing the overall gain and maintaining the dynamic range at 30 to 35 dB can minimize the "noise" resulting from the low-amplitude and relatively high-velocity signal of blood flow. Pulsed tissue Doppler velocities are generally higher than velocities measured from color tissue Doppler imaging by 10% to 20%,[119,120] and the two techniques cannot be used interchangeably to assess myocardial velocities.

The velocities of several diastolic and systolic peaks can be measured on tissue Doppler tracings of annular motion (Figure 11). Two
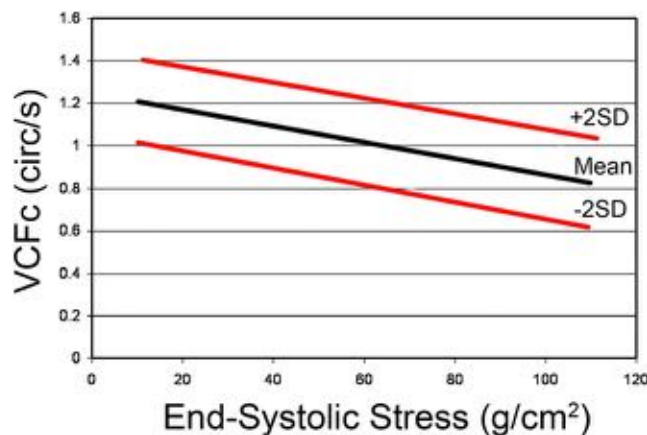
Figure 9 Relationship between the velocity of circumferential fiber shortening corrected for heart rate and LV end-systolic wall stress showing the normal ranges. *SD*, Standard deviation; *VCFc*, velocity of circumferential fiber shortening corrected for heart rate.

negative diastolic peaks occur when the annulus moves away from the apex and can usually be identified separately as early diastolic annular motion (e′ wave), which reflects ventricular recoil from a contracted state, and annular motion during atrial contraction (a′ wave), which is affected by both ventricular diastolic and atrial systolic function.[53] A positive systolic peak represents annular motion toward the apex during systole (s′ wave). IVRT′ can be measured from the end of the s′ wave to the onset of the e′ wave, and isovolumic contraction time (IVCT′) can be measured from the end of the a′ wave to the onset of the s′ wave. It is important to recognize that IVRT′ assessed by AV valve annular motion may not correlate with IVRT assessed by blood flow Doppler interrogation, particularly when diastolic dysfunction is present, because IVRT′ appears to be less influenced by filling pressures and to correlate well with τ (the LV relaxation time constant).[121] A velocity peak is frequently seen during isovolumic contraction, and the isovolumic acceleration calculated as this velocity divided by the time to peak velocity is an index of systolic function.[122] Age-related reference values of annular velocities and time intervals have been published for children and adolescents.[117,118,123-129]

Other Doppler indices of LV systolic and diastolic function have been reported. The estimated mean or peak isovolumic rate of pressure change (dP/dt) from the mitral regurgitation continuous-wave Doppler tracing has been used as a nongeometric index of LV systolic function.[130,131] The velocity ratio of the blood flow Doppler–derived mitral inflow E wave to the tissue Doppler–derived e′ wave has been used to assess LV diastolic function. Color M-mode measurements of the early diastolic flow propagation velocity from the MV to the apex correlate well with τ and provide another means by which to evaluate LV filling; as LV relaxation becomes abnormal, the rate of early diastolic flow propagation into the left ventricle decreases.[132-134] Pediatric experience with these methods is limited, and their accuracy and reproducibility in children remain unknown. The myocardial performance index, calculated as isovolumic relaxation time plus isovolumic contraction time divided by ejection time and measured either by spectral or tissue Doppler analysis, has been used to assess combined LV systolic and diastolic function, and reference values in adults and children are available.[135,136] More recently, myocardial deformation analyses with measurements of strain, strain rate, and ventricular torsion by tissue Doppler or speckle-tracking echocardiography have received attention as

Table 4 Measurements of the Left Ventricle

Measurement	Technique/View	Timing/Location	Applications	Strengths	Weaknesses
End-diastolic diameter (EDD)	2D Parasternal or subxiphoid short-axis	End-diastole* just below mitral annulus	LV size	Adjustable alignment Normal adult data[1] Normal pediatric data[15,17]	Lower temporal resolution than M-mode Inappropriate for abnormal LV shape Depends on good blood-endocardium border No normal data
End-diastolic posterior wall thickness (EDPWT)	2D Parasternal or subxiphoid short-axis	End-diastole* just below mitral annulus	LV size	Adjustable alignment Normal adult data[1] Normal pediatric data[15,17]	Same as above
End-diastolic septal wall thickness (EDSWT)	2D Parasternal or subxiphoid short-axis	End-diastole* just below mitral annulus	LV size	Adjustable alignment Normal adult data[1] Normal pediatric data[15,17]	Same as above
End-systolic diameter (ESD)	2D Parasternal or subxiphoid short-axis	End-systole† just below mitral annulus	LV size	Adjustable alignment Normal adult data[1] Normal pediatric data[15,17]	Same as above
End-systolic posterior wall thickness (ESPWT)	2D Parasternal or subxiphoid short-axis	End-systole† just below mitral annulus	LV size	Adjustable alignment Normal adult data[1] Normal pediatric data[15,17]	Same as above
End-systolic septal wall thickness (ESSWT)	2D Parasternal or subxiphoid short-axis	End-systole† just below mitral annulus	LV size	Adjustable alignment Normal adult data[1] Normal pediatric data[15,17]	Same as above
End-diastolic length (EDL)	2D Apical 4-chamber or subxiphoid long-axis	End-diastole*	LV size	Adjustable alignment Normal adult data[1] Normal pediatric data[15,17]	Foreshortening Depends on distinct apical endocardium
End-diastolic epicardial length (EDL$_{epi}$)	2D Apical 4-chamber or subxiphoid long-axis	End-diastole*	LV size	Adjustable alignment Normal adult data[1] Normal pediatric data[15,17]	Foreshortening Depends on distinct apical endocardium
End-diastolic area (EDA)	2D Parasternal or subxiphoid short-axis	End-diastole*	LV size	Adjustable alignment Normal adult data[1] Normal pediatric data[15,17]	Depends on good blood-endocardium border
End-diastolic epicardial area (EDA$_{epi}$)	2D Parasternal or subxiphoid short-axis	End-diastole*	LV size	Adjustable alignment Normal adult data[1] Normal pediatric data[15,17]	Depends on good blood-endocardium border
End-systolic length (ESL)	2D Apical 4-chamber or subxiphoid long-axis	End-systole*	LV size	Adjustable alignment Normal adult data[1] Normal pediatric data[15,17]	Foreshortening Depends on distinct apical endocardium
End-systolic epicardial length (ESL$_{epi}$)	2D Apical 4-chamber or subxiphoid long-axis	End-systole*	LV size	Adjustable alignment Normal adult data[1] Normal pediatric data[15,17]	Foreshortening Depends on distinct apical endocardium
End-systolic area (ESA)	2D Parasternal or subxiphoid short-axis	End-systole*	LV size	Adjustable alignment Normal adult data[1] Normal pediatric data[15,17]	Depends on good blood-endocardium border

(Continued)

Table 4   (*Continued*)

Measurement	Technique/View	Timing/Location	Applications	Strengths	Weaknesses
End-systolic epicardial area (ESA$_{epi}$)	2D Parasternal or subxiphoid short-axis	End-systole[†]	LV size	Adjustable alignment Normal adult data[1] Normal pediatric data[15,17]	Depends on good blood-endocardium border
Peak MV annular velocity in early diastole (e')	Tissue Doppler Apical 4-chamber	Early diastole at lateral & medial MV annulus	LV diastolic function	Reproducible Good temporal resolution Normal pediatric data[117, 118, 123-128]	Depends on alignment (angle-dependent) Depends on loading conditions Not useful for regional wall motion abnormalities
Peak MV annular velocity at atrial contraction (a')	Tissue Doppler Apical 4-chamber	Atrial contraction at lateral & medial MV annulus	LV diastolic function	Same as above	Same as above
Peak MV annular velocity in systole (s')	Tissue Doppler Apical 4-chamber	Systole at lateral & medial MV annulus	LV systolic function	Same as above	Same as above
Peak MV annular velocity in isovolumic contraction	Tissue Doppler Apical 4-chamber	Isovolumic contraction at lateral & medial MV annulus	LV systolic function	Same as above	Same as above
Isovolumic relaxation time (IVRT')[‡]	Tissue Doppler Apical 4-chamber	Time from end of s' wave to beginning of e' wave	LV diastolic function	Same as above	Same as above
Isovolumic contraction time (IVCT')	Tissue Doppler Apical 4-chamber	Time from end of a' wave to beginning of s' wave	LV systolic function	Same as above	Same as above
Time to peak velocity in isovolumic contraction	Tissue Doppler Apical 4-chamber	Isovolumic contraction at lateral & medial MV annulus	LV systolic function	Same as above	Same as above

Calculation	Technique	Formula	Applications	Strengths	Weaknesses
End-diastolic volume (EDV)	Biplane Simpson with apical 4- and 2-chamber views	Summation of disks: $\frac{\pi}{4} \times \sum_{i=1}^{N} ai \times bi \times \frac{L}{N}$	LV size	Fewer geometric assumptions than short-axis dimensions Normal adult data[1] Normal pediatric data[15]	Foreshortening Depends on good blood-endocardium border Little normal pediatric data
End-systolic volume (ESV)	Biplane Simpson with apical 4- and 2-chamber views	Same as above	LV size	Same as above	Same as above
End-diastolic epicardial volume (EDV$_{epi}$)	Biplane Simpson with apical 4- and 2-chamber views	Same as above	LV size	Same as above	Same as above
LV mass	Biplane Simpson with apical 4- and 2-chamber views	(EDV$_{epi}$ – EDV) x 1.05 g/ml	LV size	Same as above	Same as above
End-diastolic volume (EDV)	Area-length	5/6 x EDA x EDL	LV size	Same as above	Foreshortening Depends on distinct apical endocardium Depends on good blood-endocardium border Little normal pediatric data
End-systolic volume (ESV)	Area-length	5/6 x ESA x ESL	LV size	Same as above	Same as above

(*Continued*)

Table 4 (*Continued*)

Calculation	Technique	Formula	Applications	Strengths	Weaknesses
End-diastolic epicardial volume (EDV$_{epi}$)	Area-length	5/6 x EDA$_{epi}$ x EDL$_{epi}$	LV size	Same as above	Same as above
LV mass	Area-length	(EDV$_{epi}$ − EDV) x 1.05 g/ml	LV size	Same as above	Same as above
Shortening fraction (SF)	M-mode 2D	(EDD − ESD)/EDD	LV systolic function	Extensive experience Easy Normal adult data[1]	Depends on loading conditions Inappropriate for abnormal LV shape Depends on good blood-endocardium border
Ejection fraction (EF)	Biplane Simpson Area-length 3D	(EDV − ESV)/EDV	LV systolic function	Less sensitive to abnormal LV shape Normal adult data[1]	Depends on loading conditions Foreshortening Depends on distinct apical endocardium Depends on good blood-endocardium border
Velocity of circumferential fiber shortening corrected for heart rate and normalized to end-systolic wall stress	M-mode 2D	VCF = SF/ET VCF$_c$ = SF/ET$_c$ ESS = (P$_{es}$ x R$_{es}$)/T$_{es}$	LV systolic function	Independent of preload Accounts for afterload and heart rate Normal pediatric data[113]	Inappropriate for abnormal LV shape Time-consuming
Early diastolic velocity ratio	Tissue Doppler	E/e'	LV diastolic function		Depends on alignment (angle-dependent) Depends on loading conditions
Isovolumic acceleration (IVA)	Tissue Doppler	MV peak isovolumic annular velocity/time to peak velocity	LV systolic function		Same as above

a_i, Minor axis slice radius in the apical 4-chamber view; b_i, minor axis slice radius in the apical 2-chamber view; *EDA*, End-diastolic area; *EDA$_{epi}$*, end-diastolic epicardial area; *EDD*, end-diastolic diameter; *EDL*, end-diastolic length; *EDL$_{epi}$*, end-diastolic epicardial length; *EDPWT*, end-diastolic posterior wall thickness; *EDSWT*, end-diastolic septal wall thickness; *ESA*, end-systolic area; *ESA$_{epi}$*, end-systolic epicardial area; *ESD*, end-systolic diameter; *ESL*, end-systolic length; *ESL$_{epi}$*, end-systolic epicardial length; *ESPWT*, end-systolic posterior wall thickness; *ESS*, end-systolic wall stress; *ESSWT*, end-systolic septal wall thickness; *ET*, ejection time; *ET$_c$*, ET corrected for heart rate; *L*, left ventricular length; *LV*, left ventricular; *MV*, mitral valve; *N*, number of slices; *P$_{es}$*, pressure at end-systole; *R$_{es}$*, radius at end-systole; *T$_{es}$*, wall thickness at end-systole; *3D*, three-dimensional; *2D*, two-dimentional; *VCF*, velocity of circumferential fiber shortening; *VCF$_c$*, VCF corrected for heart rate.

*Maximum minor-axis diameter or area.

†Minimum minor-axis diameter or area.

‡Measured by tissue Doppler evaluation rather than by blood flow Doppler evaluation, as described in Table 3.
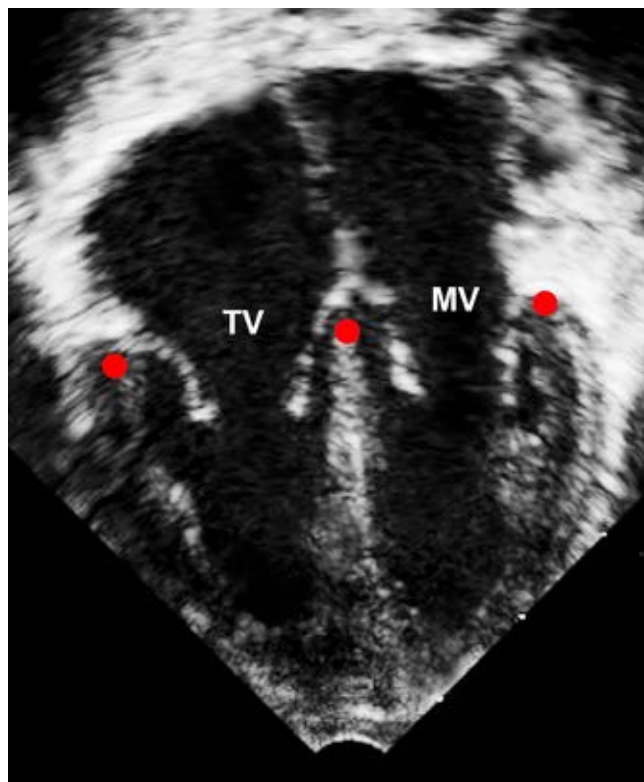
Figure 10 Apical 4-chamber view displaying 3 cursor locations for tissue Doppler evaluation. *MV*, Mitral valve; *TV*, tricuspid valve.
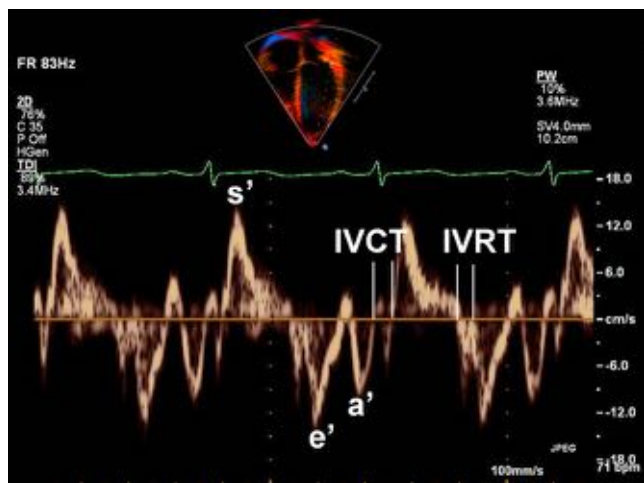
Figure 11 Lateral mitral annular tissue Doppler tracing. *a'*, Peak velocity during atrial contraction; *e'*, peak velocity during early ventricular diastole; *IVCT*, isovolumic contraction time; *IVRT*, isovolumic relaxation time; *s'*, peak velocity during ventricular systole.

potentially useful indices of LV function.[137-141] The utility of these new techniques in children deserves further study.

Recommendations (Table 4): When tissue Doppler evaluation is performed at the medial and lateral MV annulus, the recommended measurements and calculations include peak e′, a′, and s′ velocities; IVRT′; IVCT′; isovolumic acceleration; and the E/e′ ratio.

Right Ventricle

Morphometric Evaluation. Two-dimensional echocardiography has been used to assess RV size and function, though it generally underestimates RV volumes compared with MRI.[142] In addition, there are inherent limitations to the application of linear and cross-sectional area measurements to a geometrically complex chamber,[143] and the right ventricle is technically difficult to evaluate by echocardiography because of its anterior retrosternal position. Nevertheless, guidelines on the assessment of RV wall thickness, size, and systolic function in adults have been published.[1] The RV free wall thickness is difficult to quantify, though it can be measured in subxiphoid long-axis or parasternal views at end-diastole,[1,144] making sure to avoid regions with significantly coarse trabeculations. As with the left ventricle in an apical 4-chamber view, the RV basal border is defined as the line connecting the TV annular hinge points. The RV basal and midcavity minor-axis diameters and RV major-axis length can be measured at end-diastole (defined as the frame at which the TV closes), taking care not to foreshorten the right ventricle (Figure 12). Again, 2D measurements of the RV have correlated weakly with MRI measurements, especially in the setting of RV volume overload.[143]

RV long-axis area can be measured by planimetry, and RV fractional area change has been used as an index of RV systolic function.[145] Multiple formulas have been proposed to estimate RV volume by 2D echocardiography.[146-148] However, all of these methods have significant limitations, with little or no data regarding utility, accuracy, and reproducibility in children,[145] and the best method for routine 2D measurement of RV volume remains controversial. RV EF can be calculated using these volume estimation methods and is regarded as a load-dependent index of RV systolic function. However, this approach has correlated only modestly with measurements from MRI and radionuclide imaging.[149] Tricuspid annular plane systolic excursion (TAPSE) is another measure of RV systolic function that correlates well with EF as measured by radionuclide angiography and 2D echocardiography in adults.[150,151] It measures longitudinal shortening of the right ventricle in an apical 4-chamber view, usually acquired by placing an M-mode cursor through the tricuspid annulus. Published normal values for TAPSE in children are available,[152] though its clinical significance is still under investigation.

Recommendations (Table 5): The recommended methods to assess RV size include measurement of end-diastolic diameters at the basal and midcavity levels, end-diastolic length, and end-diastolic and end-systolic planimetered areas in apical 4-chamber views. The recommended methods to assess RV systolic function include TAPSE and fractional area change in apical 4-chamber views.

Doppler Evaluation. The peak velocity of the tricuspid regurgitation jet provides a good estimation of RV systolic pressure, particularly when RA pressure is low. Many of the previously described Doppler indices used to characterize LV function have been applied to the right ventricle. For example, tricuspid annular displacement measured by tissue Doppler evaluation can help assess RV systolic and diastolic function.[117,122,153-157] The dP/dt estimated from the tricuspid regurgitation continuous-wave Doppler tracing has also been used to assess RV systolic function.[149] RA pressure and RV diastolic function can be assessed by the IVC collapsibility index,[39,40] hepatic venous flow indices,[158] TV inflow velocities, the velocity ratio of TV E wave to TV e′ wave,[159,160] the velocity ratio of TV E wave to color M-mode inflow propagation,[161] and RV IVRT′.[162] In addition,
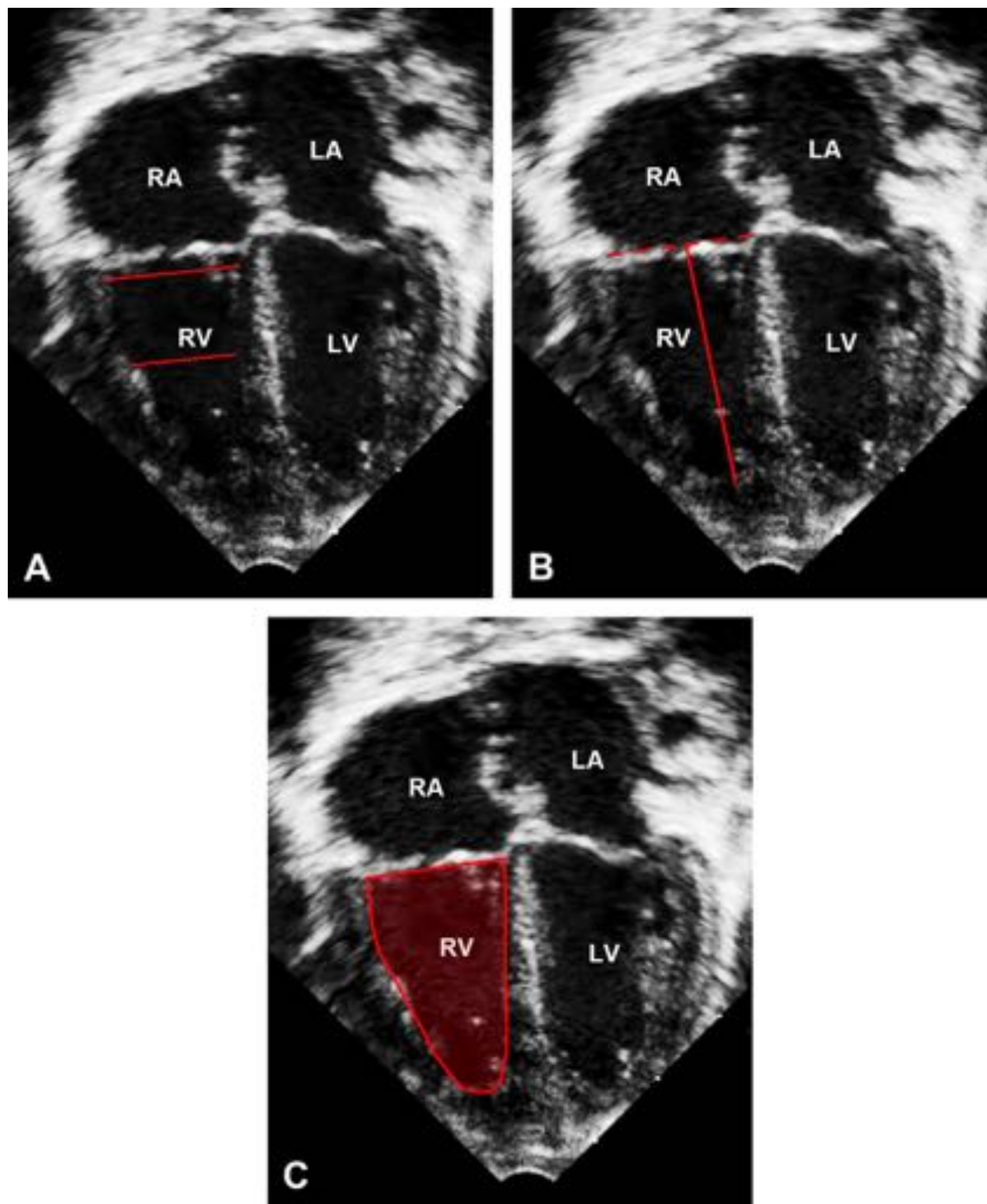
Figure 12 Apical 4-chamber view at end-diastole showing **(A)** right ventricular basal and midcavity diameters, **(B)** right ventricular length, and **(C)** right ventricular area. *LA,* Left atrium; *LV,* left ventricle; *RA,* right atrium; *RV,* right ventricle.

antegrade flow across the PV at end-diastole may suggest restrictive RV physiology.[163,164] The myocardial performance index measured by conventional or tissue Doppler evaluation has also been used to assess combined RV systolic and diastolic function.[135,136] The normal values obtained from these two approaches, however, can be significantly different,[165] and the appropriate reference values should be used. Newer methods for assessing RV systolic and diastolic function, such as speckle tracking for strain and strain rate analyses and 3D echocardiography, deserve further study.[149,166]

Table 5 Measurements of the Right Ventricle

Measurement	Technique/View	Timing/Location	Applications	Strengths	Weaknesses
End-diastolic basal diameter	2D Apical 4-chamber	End-diastole*	RV size	Normal adult data[1]	Foreshortening Difficult to visualize RV lateral wall Depends on good blood-endocardium border Depends on distinct apical endocardium Depends on loading conditions Poorly predicts RV volume measured by MRI[143] No normal pediatric data
End-diastolic mid-cavity diameter	2D Apical 4-chamber	End-diastole*	RV size	Normal adult data[1]	Same as above
End-diastolic length	2D Apical 4-chamber	End-diastole*	RV size	Normal adult data[1]	Same as above
End-diastolic area (EDA)	2D Apical 4-chamber	End-diastole*	RV size	Normal adult data[1]	Same as above
End-systolic area (ESA)	2D Apical 4-chamber	End-systole[†]	RV size	Normal adult data[1]	Same as above
Tricuspid annular plane systolic excursion (TAPSE)	M-mode Apical 4-chamber view	Tricuspid annulus	RV systolic function	Correlates to EF Quick and simple Reproducible	Normal values not adjusted for body size[152] Not evaluated in children with CHD Depends on loading conditions
Tricuspid regurgitation (TR) jet peak velocity	Apical or parasternal	Systole	Estimation of RV systolic pressure		Depends on alignment (angle-dependent) Trivial TR may not provide accurate estimate of RV pressure
Peak TV annular velocity in early diastole (e')	Tissue Doppler Apical 4-chamber	Early diastole at lateral & medial TV annulus	RV diastolic function	Reproducible Good temporal resolution Normal pediatric data[117, 118, 123, 124, 126, 127, 129]	Depends on alignment (angle-dependent) Depends on loading conditions Not useful for regional wall motion abnormalities
Peak TV annular velocity at atrial contraction (a')	Tissue Doppler Apical 4-chamber	Atrial contraction at lateral & medial TV annulus	RV diastolic function	Same as above	Same as above
Peak TV annular velocity in systole (s')	Tissue Doppler Apical 4-chamber	Systole at lateral & medial TV annulus	RV systolic function	Same as above	Same as above
Peak TV annular velocity in isovolumic contraction	Tissue Doppler Apical 4-chamber	Isovolumic contraction at lateral TV annulus	RV systolic function	Same as above	Same as above
Isovolumic relaxation time (IVRT')	Tissue Doppler Apical 4-chamber	Time from end of s' wave to beginning of e' wave	RV diastolic function	Same as above	Same as above
Time to peak velocity in isovolumic contraction	Tissue Doppler Apical 4-chamber	Isovolumic contraction at lateral TV annulus	RV systolic function	Same as above	Same as above

(Continued)

Table 5 (*Continued*)

Measurement	Technique/View	Timing/Location	Applications	Strengths	Weaknesses
Fractional area change (FAC)	2D of apical 4-chamber view	FAC = (EDA − ESA)/EDA	RV systolic function	Modestly correlates to EF by MRI[1] Normal adult data[1]	Foreshortening Difficult to visualize RV lateral wall Depends on good blood-endocardium border Depends on distinct apical endocardium Depends on loading conditions Poorly predicts EF by MRI with increased preload[143] No normal pediatric data
Isovolumic acceleration (IVA)	Tissue Doppler	IVA = TV peak isovolumic annular velocity/time to peak velocity	RV systolic function		Depends on alignment (angle-dependent) Depends on loading conditions

EDA, End-diastolic area; *EDV*, end-diastolic volume; *ESA*, end-systolic area; *ET*, ejection time across pulmonary valve; *FAC*, fractional area change; *IVA*, isovolumic acceleration; *RV*, right ventricular; *TR*, tricuspid regurgitation; *TV*, tricuspid valve; *2D*, two-dimensional.
*Maximum dimension or area.
†Minimum area.
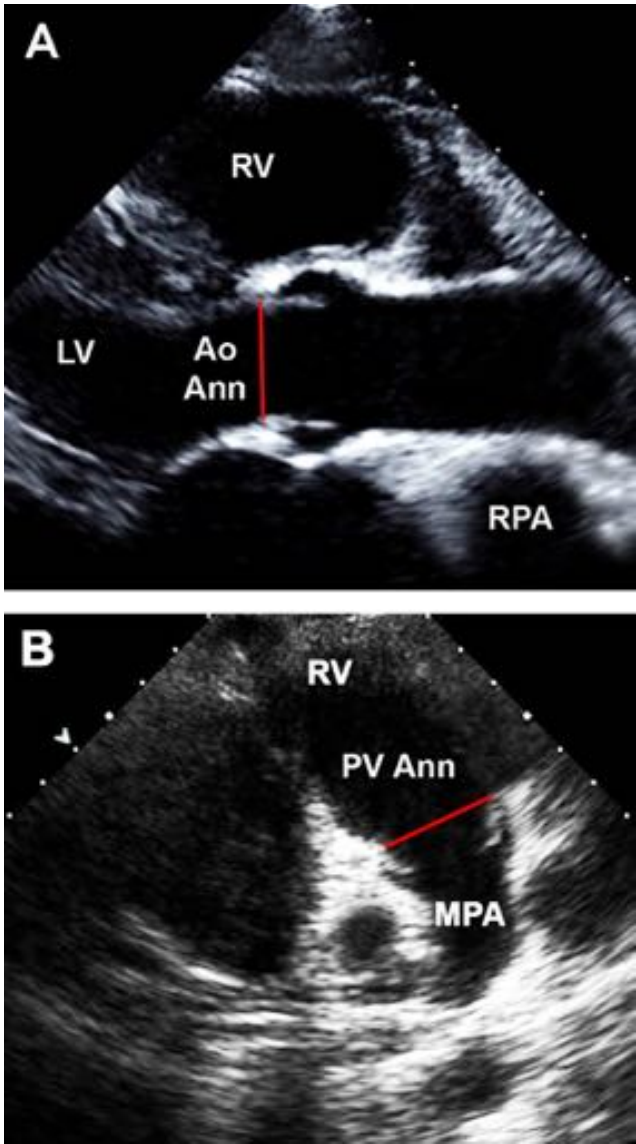
Figure 13 Parasternal long-axis views showing **(A)** aortic annular diameter (Ao Ann) and **(B)** pulmonary annular diameter (PV Ann). *LV*, Left ventricle; *MPA*, main pulmonary artery; *RPA*, right pulmonary artery; *RV*, right ventricle.

Recommendations (Table 5): When tissue Doppler evaluation is performed at the TV annulus, the recommended measurements and calculations include peak e′, a′, and s′ velocities; IVRT′; and isovolumic acceleration.

Ventricular Outflow Tracts and Semilunar Valves

Morphometric Evaluation. Subvalvar and valvar outflow tract measurements adjusted for the effects of body size help evaluate potential outflow tract hypoplasia and annular dilation. The transducer imaging plane should be parallel to the outflow tract long axis (to allow for an axial measurement of the outflow tract), and magnification of the region of interest should be used. Although the subvalvar cross-section in both outflow tracts is often elliptical in shape, a circular shape is assumed and a single diameter measured. The maximum dimension of the narrowest subvalvar LV outflow

Table 6 Measurements of the Ventricular Outflow Tracts and Semilunar Valves

Measurement	View/Location	Timing	Applications	Strengths	Weaknesses
Subvalvar LV outflow tract	Parasternal long-axis	Systole*	LV outflow tract size	Normal adult data[1]	Avoid oblique alignment Non-circular geometry
Aortic annulus diameter	Parasternal long-axis	Systole*	Aortic annulus size	Reproducibility Normal adult data[1] Normal pediatric data[15-17]	Avoid oblique alignment Non-circular geometry
Subvalvar RV outflow tract	Parasternal long- or short-axis	Systole*	RV outflow tract size	Normal adult data[1]	Avoid oblique alignment Non-circular geometry Low antero-lateral resolution
Pulmonary annulus	Parasternal long- or short-axis	Systole*	Pulmonary annulus size	Reproducibility Normal adult data[1] Normal pediatric data[15-17]	Same as above
LV outflow tract peak velocity	Apical 3-chamber, suprasternal long-axis, or right parasternal	Systole	Outflow tract obstruction		Depends on alignment Affected by ventricular systolic function
RV outflow tract peak velocity	Subxiphoid short-axis, apical 4-chamber with anterior sweep, parasternal long-axis with leftward anterior sweep, or parasternal short-axis	Systole	Outflow tract obstruction		Depends on alignment Affected by ventricular systolic function

LV, Left ventricular; *RV*, right ventricular.
*Maximum diameter.
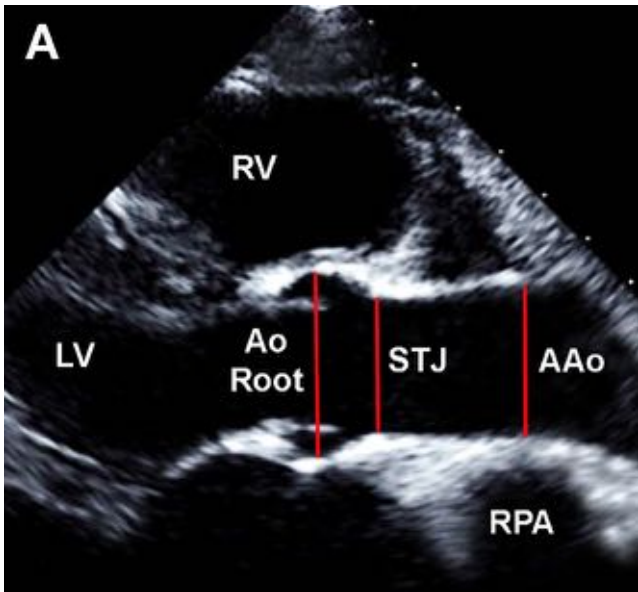
Figure 14 Aortic root (Ao Root), sinotubular junction (STJ), and ascending aorta (AAo) diameters in a parasternal long-axis view at mid-systole. *LV*, Left ventricle; *RPA*, right pulmonary artery; *RV*, right ventricle.

Figure 15 Proximal transverse arch (PTA), distal transverse arch (DTA), and aortic isthmus (AI) diameters in a suprasternal long-axis view. *LCCA*, Left common carotid artery; *LSA*, left subclavian artery; *RPA*, right pulmonary artery.

tract diameter is best measured in parasternal long-axis views during early to mid-systole, and this value has been used to calculate stroke volume and cardiac output in adults.[85] In contrast, the subvalvar RV outflow tract diameter has been variably measured in parasternal long-axis and short-axis views.[1] Reference values for subvalvar diam-

eters along both outflow tracts are available in adults.[1] Data on the utility, accuracy, and reproducibility of these measurements in children are scant.
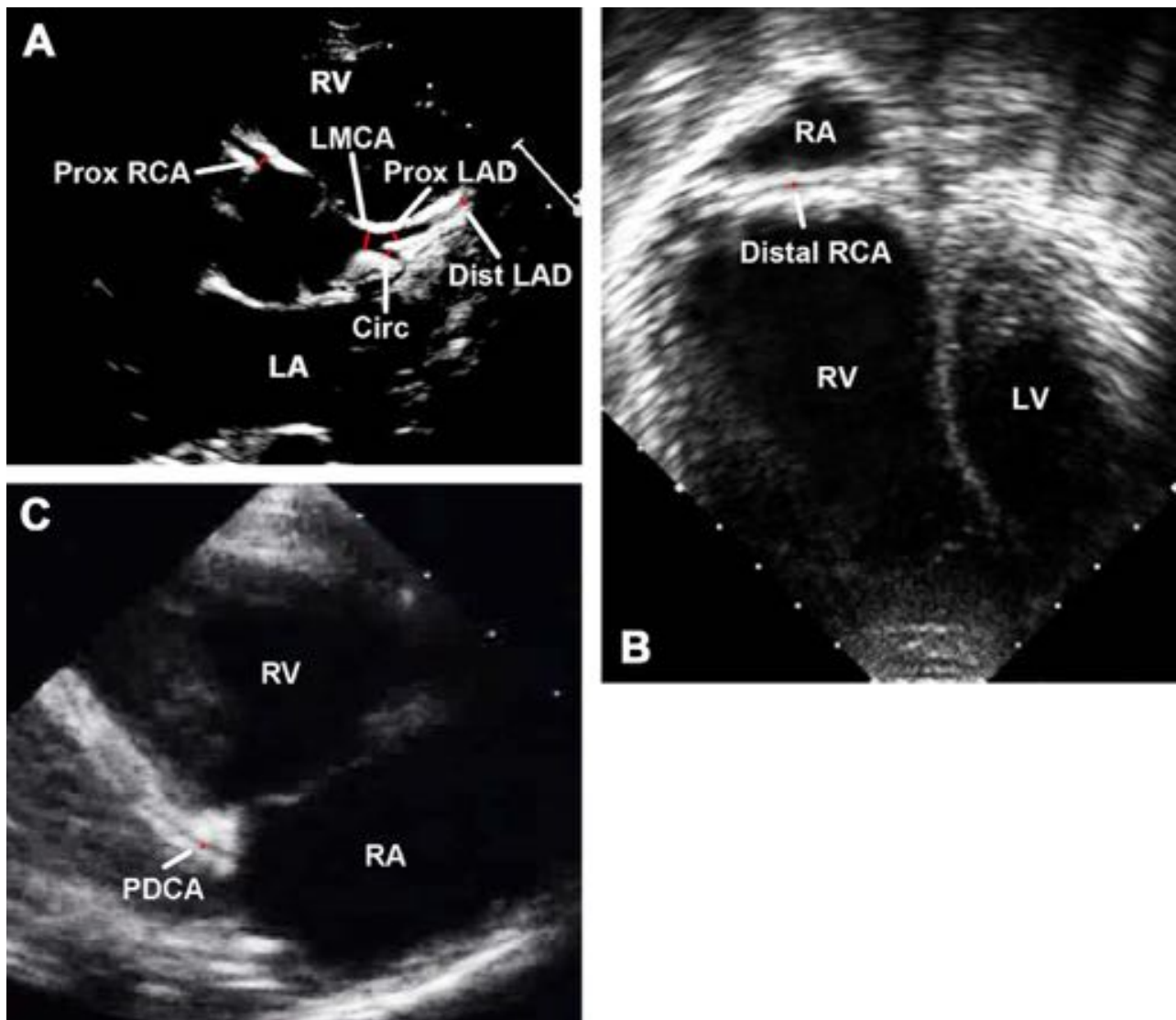
Figure 16 **(A)** Left main coronary artery (LMCA), proximal left anterior descending coronary artery (Prox LAD), distal left anterior descending coronary artery (Dist LAD), circumflex coronary artery (Circ), and proximal right coronary artery (Prox RCA) diameters in a parasternal short-axis view; **(B)** distal right coronary artery (Distal RCA) diameter in an apical 4-chamber view with posterior angulation; and **(C)** posterior descending coronary artery (PDCA) diameter in a parasternal long-axis view with posterior angulation. *LA*, Left atrium; *LV*, left ventricle; *RA*, right atrium; *RV*, right ventricle.

AoV and PV annular diameters are best measured with magnification in parasternal long-axis views from the inner edge of the proximal valve insertion hinge point within the arterial root to the inner edge of the opposite hinge point (Figure 13). As with the subvalvar RV outflow tract, PV annular and main pulmonary artery diameters can also be measured in parasternal short-axis views. However, these measurements are often underestimated because they rely on the lateral imaging plane, with its relatively low resolution,[167] and because an oblique orientation is often the only one available in these views. Both annular diameters have been measured at variable times during the cardiac cycle. For example, measurements of the aortic annulus and root in diastole have been recommended for children and adults,[12] and reference values are available.[13] However, systolic values for annular diameters appear to correlate best with intraoperative measurements.[168] In addition, outflow tract imaging during mid-systole provides more consistent display of valve hinge points and intraluminal diameters, which in turn can be used to calculate stroke volume and cardiac output. Therefore, AoV and PV annular measurements during mid-systole are recommended in children.

Recommendations (Table 6): The diameters of the subvalvar LV outflow tract and aortic annulus are best measured in parasternal long-axis views during early to mid-systole. The diameters of the subvalvar RV outflow tract and pulmonary annulus can be measured in parasternal long-axis or short-axis views during mid-systole, using the largest diameters for documentation.

Doppler Evaluation. Doppler interrogation of the LV outflow tract is usually performed in apical 3-chamber, right parasternal, or suprasternal long-axis views, whereas the RV outflow tract can be interrogated in parasternal long-axis, subxiphoid short-axis, or modified
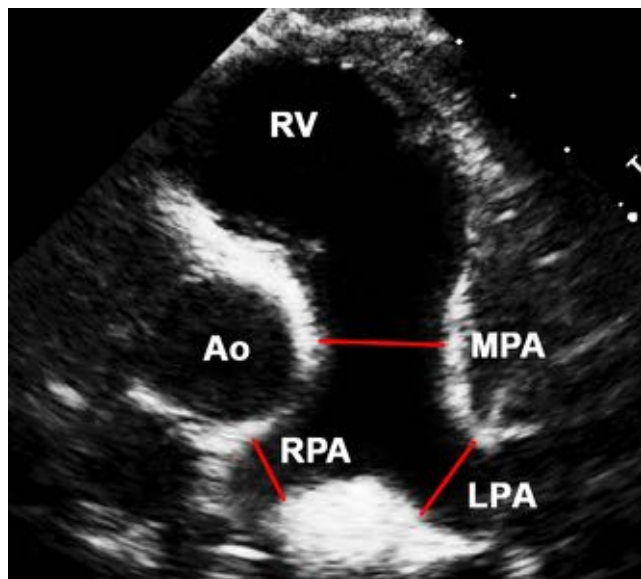
Figure 17 Main pulmonary artery (MPA) and proximal branch pulmonary artery diameters in a parasternal short-axis view. *Ao*, Aorta; *LPA*, left pulmonary artery; *RPA*, right pulmonary artery; *RV*, right ventricle.

apical views with anterior angulation. The measured velocity can vary significantly from one view to another, especially because the geometry and orientation of the outflow tracts may vary significantly among different patients, so the view used for the measurement should always be included in the report to maintain consistency in subsequent studies. Recommendations from the ASE and the European Association of Echocardiography on the quantification of AoV and PV stenosis in adults are available.[76] The severity of total subvalvar and valvar outflow tract obstruction is usually determined from measurement of the maximum instantaneous and mean gradients by continuous-wave Doppler interrogation, and the cleanest and highest velocity spectral Doppler envelope should be used.[169] Pulsed-wave Doppler interrogation using a low-frequency transducer can sometimes evaluate the contribution of subvalvar stenosis in the setting of multiple levels of obstruction, though it is important to remember that the dominant resistor of stenoses in series always masks the hemodynamic effects of the more distal levels of obstruction.[170] In the setting of marked ventricular dysfunction and consequently low cardiac output, the Doppler-derived gradient does not always represent the severity of the obstruction. In fact, a modest gradient with significant ventricular systolic dysfunction should be considered as relatively severe stenosis. In addition, the severity of PV stenosis may not be accurately assessed when a large ventricular septal defect or patent ductus arteriosus results in equalization of ventricular and arterial pressures. In the setting of ventricular dysfunction or a large shunting lesion, abnormalities in semilunar valvar morphology (thickening, doming, commissural fusion) and annular size are as useful as the Doppler-derived gradient in assessing severity.

The maximum instantaneous gradient measured by Doppler echocardiography is different from the peak-to-peak gradient measured by catheterization, partially secondary to pressure recovery,[171] a phenomenon that is particularly important in children. More severe degrees of aortic stenosis and a larger ascending aorta relative to annular size result in more turbulence and less pressure recovery. Because the ascending aorta is frequently less dilated in children with aortic stenosis compared with adults, pressure recovery can

contribute substantially to the difference between Doppler-derived gradients and those obtained by catheterization, resulting in differences as high as 20% to 40%.[171-174] The effective orifice area across a diseased valve can also help assess the degree of valvar stenosis,[169,175] and valvar area can be measured by 2D planimetry or calculated by using the continuity equation, as described for the AV valves. Similar to the problems with the MV and TV, 2D planimetry of AoV and PV area is usually unreliable because of the irregular funnel-like doming of the stenotic valve and the difficulty with obtaining a reliable "en face" view of the true leaflet opening. The continuity equation also permits calculation of the AoV area,[175] though measurements of the subvalvar LV outflow tract diameter can vary by as much as 5% to 8% in adults.[176] This variability is exaggerated in the pediatric population, in which the smaller elliptical subvalvar cross-sectional area may increase the potential for error, thereby precluding routine use of this approach in children with small outflow tracts and semilunar valves. Quantitative assessment of AoV and PV regurgitation has also been discussed previously for adults,[81] and the utility of vena contracta diameter and regurgitant jet area as well as the continuity equation and proximal isovelocity surface area phenomenon in children are limited and have not been validated.

Recommendations (Table 6): The maximum instantaneous and mean gradients along the LV outflow tract are best measured in apical 3-chamber, suprasternal long-axis, or right parasternal views. The gradients along the RV outflow tract are best measured in subxiphoid short-axis, modified apical 4-chamber, parasternal long-axis, or parasternal short-axis views.

Aorta, Coronary Arteries, and Pulmonary Arteries

Morphometric Evaluation. Measurement of arterial vessels helps identify patients with diverse vascular abnormalities, such as Marfan syndrome and Kawasaki disease.[1-5,13,177-181] The timing of the measurement during the cardiac cycle has been discussed extensively. Some have recommended performing the measurement during either diastole or systole or using an average of both measurements,[182] though systolic diameters are in fact significantly larger than diastolic diameters.[183,184] In addition, the maximum effect of vascular size on vessel function occurs during peak flow, and peak wall stress at the time of peak systolic pressure is the primary determinant of dissection or rupture in patients with aortic dilation. All measurements of the arterial vessels in children should be made at the moment of maximum expansion, typically at peak flow during mid-systole.

The proximal aorta is frequently dilated in the setting of a connective tissue disease (such as Marfan syndrome) or a bicuspid AoV.[3,5,33,177,185-187] In contrast, narrowing at the sinotubular junction associated with supravalvar aortic stenosis is frequently seen in the setting of Williams syndrome.[188] The proximal aorta should be measured at the following levels in a parasternal long-axis view at the moment of maximum expansion: the aortic root at the sinuses of Valsalva, the sinotubular junction, and the ascending aorta as it crosses in front of the right pulmonary artery (Figure 14). Optimal imaging of the entire proximal aorta is not always available in the standard parasternal window, and a high left parasternal view located one or two rib interspaces superior to the standard location may be required. Often, a high right parasternal view in a right lateral decubitus position is better at displaying the entire proximal aorta. After the aortic arch sidedness has been established and the branches identified in

Table 7 Measurements of the Aorta, Coronary Arteries, and Pulmonary Arteries

Measurement	View/Location	Timing	Applications	Strengths	Weaknesses
Aortic root diameter	Parasternal long-axis, high left parasternal, or high right parasternal	Systole*	Proximal aorta size	Normal adult data[1] Normal pediatric data[15,17]	May not reflect largest diameter in abnormally shaped aortic roots[192] Depends on alignment
Aortic sino-tubular junction diameter	Parasternal long-axis, high left parasternal, or high right parasternal	Systole*	Proximal aorta size	Same as above	Same as above
Ascending aorta diameter	Parasternal long-axis, high left parasternal, or high right parasternal at level of RPA	Systole*	Proximal aorta size	Same as above	Same as above
Proximal transverse arch diameter	Suprasternal long-axis between RCCA and LCCA	Systole*	Aortic arch size	Same as above	Same as above
Distal transverse arch diameter	Suprasternal long-axis between LCCA and RSA	Systole*	Aortic arch size	Same as above	Same as above
Aortic isthmus diameter	Suprasternal long-axis distal to RSA	Systole[a]	Aortic arch size	Same as above	Same as above
Descending aorta diameter	Subxiphoid short-axis at level of diaphragm	Systole*	Descending aorta size		No normal pediatric data
Left main coronary artery (CA) diameter	Parasternal short-axis	Maximum diameter	Coronary artery size	Normal pediatric data[36]	Depends on good spatial & contrast resolution
Proximal left anterior descending CA diameter	Parasternal short-axis	Maximum diameter	Coronary artery size	Normal pediatric data[36]	Depends on good spatial & contrast resolution
Distal left anterior descending CA diameter	Parasternal short-axis	Maximum diameter	Coronary artery size		Depends on good spatial & contrast resolution
Left circumflex CA diameter	Parasternal short-axis	Maximum diameter	Coronary artery size	Normal pediatric data[36]	Depends on good spatial & contrast resolution
Proximal right CA diameter	Parasternal short-axis	Maximum diameter	Coronary artery size	Normal pediatric data[36]	Depends on good spatial & contrast resolution
Distal right CA diameter	Apical 4-chamber with posterior sweep	Maximum diameter	Coronary artery size		Depends on good spatial & contrast resolution
Posterior descending CA diameter	Parasternal long-axis with rightward posterior sweep	Maximum diameter	Coronary artery size		Depends on good spatial & contrast resolution
Main pulmonary artery (MPA) diameter	Parasternal short-axis	Systole*	Pulmonary artery size	Normal adult data[1] Normal pediatric data[15,17]	Incomplete visualization secondary to anterior location
Right pulmonary artery (RPA) diameter	Parasternal, high left parasternal, or suprasternal short-axis	Systole*	Pulmonary artery size	Normal adult data[1] Normal pediatric data[15,17]	Incomplete visualization secondary to anterior location

(Continued)

Table 7 (*Continued*)

Measurement	View/Location	Timing	Applications	Strengths	Weaknesses
Left pulmonary artery (LPA) diameter	Parasternal, high left parasternal, or suprasternal short-axis	Systole*	Pulmonary artery size	Normal adult data[1] Normal pediatric data[15,17]	Incomplete visualization secondary to anterior location
Ascending aorta peak velocity	Apical 3-chamber, suprasternal long-axis, or right parasternal	Systole	Aortic outflow tract obstruction		Depends on alignment Difficult with multiple levels of obstruction
Aortic isthmus peak velocity	Suprasternal long-axis	Systole	Aortic arch obstruction		Requires correction for proximal velocity Depends on alignment Affected by PDA
Abdominal aortic Doppler	Subxiphoid short-axis at level of diaphragm		Aortic arch obstruction Diastolic reversal from aortic regurgitation or aortic fistulous connection		
MPA peak velocity	Parasternal short-axis or apical 4-chamber with anterior sweep	Systole	Pulmonary outflow tract obstruction		Depends on alignment Difficult with multiple levels of obstruction
RPA and LPA peak velocity	Parasternal or suprasternal short-axis or high left parasternal	Systole	Branch pulmonary artery obstruction		Depends on alignment Difficult with multiple levels of obstruction

CA, Coronary artery; *LCCA*, left common carotid artery; *LPA*, left pulmonary artery; *MPA*, main pulmonary artery; *PDA*, patent ductus arteriosus; *RCCA*, right common carotid artery; *RPA*, right pulmonary artery; *RSA*, right subclavian artery.
*Maximum diameter.

a suprasternal short-axis sweep, the aortic arch is measured in a suprasternal long-axis view, though a modified high right parasternal view is occasionally better, particularly in neonates. Measurements should be performed at the following levels: the proximal transverse arch (between the innominate and left common carotid arteries), the distal transverse arch (between the left common carotid and left subclavian arteries), and the aortic isthmus (narrowest aortic segment distal to the left subclavian artery) (Figure 15). In addition, the descending aorta may be measured in a subxiphoid short-axis view at the level of the diaphragm.

The coronary arteries may become dilated with increased flow or inflammation.[189,190] They are often difficult to image in a single 2D plane. Measurements should be made at the moment of maximum expansion. Low-scale color mapping with dual display should be used when possible to avoid erroneous measurement of cardiac veins or artifacts that resemble the coronary arteries, a particular problem with the anterior and posterior descending coronary arteries. Parasternal short-axis views should be used to measure the left main, proximal and distal left anterior descending, circumflex, and proximal right coronary arteries (Figure 16). Occasionally, the left anterior descending coronary artery is better visualized in a parasternal long-axis or a modified parasternal view (between the long-axis and short-axis views). The distal right coronary artery is best seen along the right posterior AV groove in modified apical views with posterior angulation, and the posterior descending coronary artery is best seen along the posterior interventricular groove in

modified parasternal long-axis views with rightward posterior angulation.

Assessment of pulmonary artery size is important in children with various forms of CHD.[180,182,191] When pulmonary arterial flow is diminished (as in tetralogy of Fallot), the branch pulmonary arteries are typically small. In contrast, isolated PV stenosis, tetralogy of Fallot with a dysplastic PV, Marfan syndrome, and pulmonary hypertension are all associated with pulmonary artery dilation. The pulmonary arteries can be evaluated in parasternal or suprasternal short-axis views, though suprasternal measurements exhibit less variability, presumably because of less translational cardiac motion in this view.[183] The diameters of the main pulmonary artery (between the pulmonary sinotubular junction and bifurcation) and the branch pulmonary arteries can be measured in a parasternal short-axis view (Figure 17). The right pulmonary artery can also be measured as it crosses behind the ascending aorta in a suprasternal short-axis view, whereas the left pulmonary artery can also be measured at its origin from the main pulmonary artery in a left anterior oblique or sagittal plane in a suprasternal or high left parasternal ("ductal") view.

Recommendations (Table 7[192]): The proximal aortic diameters at the levels of the aortic root, sinotubular junction, and ascending aorta are best measured during mid-systole in parasternal long-axis, high left parasternal, or high right parasternal views; the proximal and distal transverse arch and aortic isthmus diameters are best measured during mid-systole in suprasternal long-axis views; and the

descending aorta diameter is best measured during mid-systole in subxiphoid short-axis views at the level of the diaphragm. The left main, proximal and distal left anterior descending, circumflex, and proximal right coronary artery diameters are best measured at the moment of maximum expansion in parasternal short-axis views; the distal right coronary artery diameter is best measured at the moment of maximum expansion in apical 4-chamber views with posterior angulation; and the posterior descending coronary artery diameter is best measured at the moment of maximum expansion in parasternal long-axis views with rightward posterior angulation. The main, right, and left pulmonary artery diameters are best measured during mid-systole in parasternal, high left parasternal, or suprasternal short-axis views.

Doppler Evaluation. Doppler evaluation of vascular structures helps identify and characterize obstruction. Similar to the AoV, Doppler interrogation of the proximal aorta is best performed in apical 3-chamber, right parasternal, or suprasternal long-axis views. The aortic arch should be evaluated in a suprasternal long-axis view with step-by-step pulsed-wave Doppler interrogation from the proximal transverse arch to the proximal descending aorta. The flow velocity in the distal transverse arch is usually too high to be ignored in the simplified Bernoulli equation, so calculated gradients along the arch should account for the proximal velocity. Pulsed-wave Doppler interrogation of the abdominal aorta in a subxiphoid short-axis view (displaying the abdominal aorta long axis) just below the diaphragm often gives the first clue that aortic arch obstruction exists. The normal pattern reveals a brisk upstroke and return to baseline, and blunting with delayed or no return to baseline is an important indicator of significant obstruction proximal to the sample site. In addition, the normal abdominal aortic Doppler pattern often reveals a brief early diastolic flow reversal secondary to aortic recoil and coronary artery flow, and holodiastolic flow reversal suggests a large aortopulmonary shunt (such as a patent ductus arteriosus) or significant aortic regurgitation.

Doppler interrogation of the main pulmonary artery is best performed in parasternal short-axis views or modified apical views with anterior angulation. In normal neonates, the branch pulmonary arteries are frequently relatively narrow, often originating from the main pulmonary artery at a slightly more acute angle. The associated flow acceleration along the proximal branch pulmonary arteries results in a benign murmur which typically resolves by 3 to 4 months of age. Standard protocols involve pulsed-wave Doppler interrogation at the origin of each branch. The line of interrogation should be parallel to the axis of the branch pulmonary arteries, and this is best performed in parasternal or suprasternal short-axis views or in a high left parasternal transverse view ("pant-leg" view). Occasionally, a modified left subclavicular view will provide the best angle of interrogation along the proximal right pulmonary artery. In contrast, Doppler interrogation of the proximal left pulmonary artery is often better performed in a high left parasternal or sagittal ("ductal") view.

Recommendations (Table 7): The abdominal aortic Doppler pattern is best evaluated in subxiphoid short-axis views. The maximum instantaneous gradient along the ascending aorta is best measured in apical 3-chamber, suprasternal long-axis, or right parasternal views. The maximum instantaneous gradient along the aortic isthmus is best measured in suprasternal long-axis views

and should account for the proximal velocity along the transverse aortic arch. The maximum instantaneous gradient along the main pulmonary artery is best measured in parasternal short-axis or modified apical views with anterior angulation. The maximum instantaneous gradient along the right and left pulmonary arteries is best measured in parasternal or suprasternal short-axis or high left parasternal views.

CONCLUSIONS AND LIMITATIONS

Quantification in pediatric echocardiography requires a consensus on what and how measurements should be made in a standard protocol, and this document has been constructed as a "manual of operations" to address this need. Although it presents a comprehensive list of guidelines when performing measurements during a pediatric echocardiogram, there are several limitations to this document. First, it does not explore the relative value of each measurement as it pertains to prognosis and outcome and therefore does not represent a list of measurements which should be performed on the basis of accuracy, reproducibility, and prognostic importance. In addition, it does not provide guidelines on how the measurements should be included in an echocardiographic report, especially in this era of structured reporting. Last, it does not fully address measurements obtained by 3D echocardiography and myocardial deformation analysis, two techniques that are currently undergoing extensive evaluation and will likely play an important role in clinical practice. This document, however, does standardize quantification methods as the first step in the task of generating a normative database that encompasses the range of body sizes and ages encountered in the pediatric population.

NOTICE AND DISCLAIMER

This report is made available by the ASE as a courtesy reference source for its members. This report contains recommendations only and should not be used as the sole basis to make medical practice decisions or for disciplinary action against any employee. The statements and recommendations contained in this report are based primarily on the opinions of experts, rather than on scientifically verified data. The ASE makes no express or implied warranties regarding the completeness or accuracy of the information in this report, including the warranty of merchantability or fitness for a particular purpose. In no event shall the ASE be liable to you, your patients, or any other third parties for any decision made or action taken by you or such other parties in reliance on this information. Nor does your use of this information constitute the offering of medical advice by the ASE or create any physician-patient relationship between the ASE and your patients or anyone else.

REFERENCES

1. Lang RM, Bierig M, Devereux RB, Flachskampf FA, Foster E, Pellikka PA, et al. Recommendations for chamber quantification: a report from the American Society of Echocardiography's Guidelines and Standards Committee and the Chamber Quantification Writing Group, developed in conjunction with the European Association of Echocardiography, a branch of the European Society of Cardiology. J Am Soc Echocardiogr 2005;18:1440-63.
2. Rozendaal L, Groenink M, Naeff MS, Hennekam RC, Hart AA, van der Wall EE, et al. Marfan syndrome in children and adolescents: an

adjusted nomogram for screening aortic root dilatation. Heart 1998;79:69-72.

3. Groenink M, Rozendaal L, Naeff MS, Hennekam RC, Hart AA, van der Wall EE, et al. Marfan syndrome in children and adolescents: predictive and prognostic value of aortic root growth for screening for aortic complications. Heart 1998;80:163-9.

4. Mart CR, Khan SA, Smith FC, Kavey RE. A new on-line method for predicting aortic root dilatation during two-dimensional echocardiography in pediatric patients with Marfan syndrome using the sinus of Valsalva to annulus ratio. Pediatr Cardiol 2003;24:118-21.

5. Aburawi EH, O'Sullivan J. Relation of aortic root dilatation and age in Marfan's syndrome. Eur Heart J 2007;28:376-9.

6. Ahmad M, Hallidie-Smith KA. Assessment of left-to-right shunt and left ventricular function in isolated ventricular septal defect. Echocardiographic study. Br Heart J 1979;41:147-58.

7. Lindstedt L, Schaeffer PJ. Use of allometry in predicting anatomical and physiological parameters of mammals. Lab Anim 2002;36:1-19.

8. Batterham AM, George KP, Whyte G, Sharma S, McKenna W. Scaling cardiac structural data by body dimensions: a review of theory, practice, and problems. Int J Sports Med 1999;20:495-502.

9. George K, Sharma S, Batterham A, Whyte G, McKenna W. Allometric analysis of the association between cardiac dimensions and body size variables in 464 junior athletes. Clin Sci (Lond) 2001;100:47-54.

10. Neilan TG, Pradhan AD, Weyman AE. Derivation of a size-independent variable for scaling of cardiac dimensions in a normal adult population. J Am Soc Echocardiogr 2008;21:779-85.

11. Lai WW, Geva T, Shirali GS, Frommelt PC, Humes RA, Brook MM, et al. Guidelines and standards for performance of a pediatric echocardiogram: a report from the Task Force of the Pediatric Council of the American Society of Echocardiography. J Am Soc Echocardiogr 2006;19:1413-30.

12. Sahn DJ, DeMaria A, Kisslo J, Weyman A. Recommendations regarding quantitation in M-mode echocardiography: results of a survey of echocardiographic measurements. Circulation 1978;58:1072-83.

13. Roman MJ, Devereux RB, Kramer-Fox R, O'Loughlin J. Two-dimensional echocardiographic aortic root dimensions in normal children and adults. Am J Cardiol 1989;64:507-12.

14. Picard MH. M-mode echocardiography: principles and examination techniques. In: Weyman AE, editor. Principles and practice of echocardiography. 2nd ed. Philadelphia: Lea & Febiger; 1994. pp. 282-301.

15. Sluysmans T, Colan SD. Theoretical and empirical derivation of cardiovascular allometric relationships in children. J Appl Physiol 2005;99:445-57.

16. Zilberman MV, Khoury PR, Kimball RT. Two-dimensional echocardiographic valve measurements in healthy children: gender-specific differences. Pediatr Cardiol 2005;26:356-60.

17. Pettersen MD, Du W, Skeens ME, Humes RA. Regression equations for calculation of z scores of cardiac structures in a large cohort of healthy infants, children, and adolescents: an echocardiographic study. J Am Soc Echocardiogr 2008;21:922-34.

18. Quinones MA, Otto CM, Stoddard M, Waggoner A, Zoghbi WA. Recommendations for quantification of Doppler echocardiography: a report from the Doppler Quantification Task Force of the Nomenclature and Standards Committee of the American Society of Echocardiography. J Am Soc Echocardiogr 2002;15:167-84.

19. Hanseus K, Bjorkhem G, Lundstrom NR. Dimensions of cardiac chambers and great vessels by cross-sectional echocardiography in infants and children. Pediatr Cardiol 1988;9:7-15.

20. DuBois D, DuBois EF. A formula to estimate the approximate surface area if height and weight be known. Arch Intern Med 1916;17:863-71.

21. Haycock GB, Schwartz GJ, Wisotsky DH. Geometric method for measuring body surface area: a height-weight formula validated in infants, children, and adults. J Pediatr 1978;93:62-6.

22. Dreyer G, Ray W. Further experiments upon the blood volume of mammals and its relation to the surface area of the body. Phil Trans R Soc Lond 1912;202:191-212.

23. Boyd E. The growth of the surface area of the human body. Minneapolis: University of Minnesota Press; 1935.

24. Cayler GG, Rudolph AM, Nadas AS. Systemic blood flow in infants and children with and without heart disease. Pediatrics 1963;32:186-201.

25. Graham TP Jr., Jarmakani JM, Canent RV Jr., Morrow MN. Left heart volume estimation in infancy and childhood. Reevaluation of methodology and normal values. Circulation 1971;43:895-904.

26. Epstein ML, Goldberg SJ, Allen HD, Konecke L, Wood J. Great vessel, cardiac chamber, and wall growth patterns in normal children. Circulation 1975;51:1124-9.

27. Roge CL, Silverman NH, Hart PA, Ray RM. Cardiac structure growth pattern determined by echocardiography. Circulation 1978;57:285-90.

28. Henry WL, Gardin JM, Ware JH. Echocardiographic measurements in normal subjects from infancy to old age. Circulation 1980;62:1054-61.

29. Abbott RD, Gutgesell HP. Effects of heteroscedasticity and skewness on prediction in regression: modeling growth of the human heart. Methods Enzymol 1994;240:37-51.

30. Gutgesell HP, Rembold CM. Growth of the human heart relative to body surface area. Am J Cardiol 1990;65:662-8.

31. Daubeney PE, Blackstone EH, Weintraub RG, Slavik Z, Scanlon J, Webber SA. Relationship of the dimension of cardiac structures to body size: an echocardiographic study in normal infants and children. Cardiol Young 1999;9:402-10.

32. Kampmann C, Wiethoff CM, Wenzel A, Stolz G, Betancor M, Wippermann CF, et al. Normal values of M mode echocardiographic measurements of more than 2000 healthy infants and children in central Europe. Heart 2000;83:667-72.

33. Warren AE, Boyd ML, O'Connell C, Dodds L. Dilatation of the ascending aorta in paediatric patients with bicuspid aortic valve: frequency, rate of progression and risk factors. Heart 2006;92:1496-500.

34. McCrindle BW, Li JS, Minich LL, Colan SD, Atz AM, Takahashi M, et al. Coronary artery involvement in children with Kawasaki disease: risk factors from analysis of serial normalized measurements. Circulation 2007;116:174-9.

35. Foster BJ, Mackie AS, Mitsnefes M, Ali H, Mamber S, Colan SD. A novel method of expressing left ventricular mass relative to body size in children. Circulation 2008;117:2769-75.

36. Olivieri L, Arling B, Friberg M, Sable C. Coronary artery Z score regression equations and calculators derived from a large heterogeneous population of children undergoing echocardiography. J Am Soc Echocardiogr 2009;22:159-64.

37. Krause I, Birk E, Davidovits M, Cleper R, Blieden L, Pinhas L, et al. Inferior vena cava diameter: a useful method for estimation of fluid status in children on haemodialysis. Nephrol Dial Transplant 2001;16:1203-6.

38. Leunissen KM, Kouw P, Kooman JP, Cheriex EC, deVries PM, Donker AJ, et al. New techniques to determine fluid status in hemodialyzed patients. Kidney Int Suppl 1993;41:S50-6.

39. Moreno FL, Hagan AD, Holmen JR, Pryor TA, Strickland RD, Castle CH. Evaluation of size and dynamics of the inferior vena cava as an index of right-sided cardiac function. Am J Cardiol 1984;53:579-85.

40. Kircher BJ, Himelman RB, Schiller NB. Noninvasive estimation of right atrial pressure from the inspiratory collapse of the inferior vena cava. Am J Cardiol 1990;66:493-6.

41. Hirata T, Wolfe SB, Popp RL, Helmen CH, Feigenbaum H. Estimation of left atrial size using ultrasound. Am Heart J 1969;78:43-52.

42. Schabelman S, Schiller NB, Silverman NH, Ports TA. Left atrial volume estimation by two-dimensional echocardiography. Cathet Cardiovasc Diagn 1981;7:165-78.

43. Wang Y, Gutman JM, Heilbron D, Wahr D, Schiller NB. Atrial volume in a normal adult population by two-dimensional echocardiography. Chest 1984;86:595-601.

44. Ujino K, Barnes ME, Cha SS, Langins AP, Bailey KR, Seward JB, et al. Two-dimensional echocardiographic methods for assessment of left atrial volume. Am J Cardiol 2006;98:1185-8.

45. Menon SC, Ackerman MJ, Cetta F, O'Leary PW, Eidem BW. Significance of left atrial volume in patients < 20 years of age with hypertrophic cardiomyopathy. Am J Cardiol 2008;102:1390-3.

46. Keller AM, Gopal AS, King DL. Left and right atrial volume by freehand three-dimensional echocardiography: in vivo validation using magnetic resonance imaging. Eur J Echocardiogr 2000;1:55-65.

47. Bommer W, Weinert L, Neumann A, Neef J, Mason DT, DeMaria A. Determination of right atrial and right ventricular size by two-dimensional echocardiography. Circulation 1979;60:91-100.

48. Schnittger I, Gordon EP, Fitzgerald PJ, Popp RL. Standardized intracardiac measurements of two-dimensional echocardiography. J Am Coll Cardiol 1983;2:934-8.

49. Bustamante-Labarta M, Perrone S, De La Fuente RL, Stutzbach P, De La Hoz RP, Torino A, et al. Right atrial size and tricuspid regurgitation severity predict mortality or transplantation in primary pulmonary hypertension. J Am Soc Echocardiogr 2002;15:1160-4.

50. Muller H, Burri H, Lerch R. Evaluation of right atrial size in patients with atrial arrhythmias: comparison of 2D versus real time 3D echocardiography. Echocardiography 2008;25:617-23.

51. Reynolds T, Appleton CP. Doppler flow velocity patterns of the superior vena cava, inferior vena cava, hepatic vein, coronary sinus, and atrial septal defect: a guide for the echocardiographer. J Am Soc Echocardiogr 1991;4:503-12.

52. Weyman AE. Right ventricular inflow tract. In: Weyman AE, editor. Principles and practice of echocardiography. 2nd ed. Philadelphia: Lea & Febiger; 1994. pp. 824-62.

53. Nagueh SF, Appleton CP, Gillebert TC, Marino PN, Oh JK, Smiseth OA, et al. Recommendations for the evaluation of left ventricular diastolic function by echocardiography. J Am Soc Echocardiogr 2009;22:107-33.

54. Klein AL, Tajik AJ. Doppler assessment of pulmonary venous flow in healthy subjects and in patients with heart disease. J Am Soc Echocardiogr 1991;4:379-92.

55. Klein AL, Stewart WJ, Bartlett J, Cohen GI, Kahan F, Pearce G, et al. Effects of mitral regurgitation on pulmonary venous flow and left atrial pressure: an intraoperative transesophageal echocardiographic study. J Am Coll Cardiol 1992;20:1345-52.

56. Stierle U, Kruger D, Mitusch R, Potratz J, Taubert G, Sheikhzadeh A. Adverse pacemaker hemodynamics evaluated by pulmonary venous flow monitoring. Pacing Clin Electrophysiol 1995;18:2028-34.

57. Rossvoll O, Hatle LK. Pulmonary venous flow velocities recorded by transthoracic Doppler ultrasound: relation to left ventricular diastolic pressures. J Am Coll Cardiol 1993;21:1687-96.

58. Yamamoto K, Nishimura RA, Burnett JC Jr., Redfield MM. Assessment of left ventricular end-diastolic pressure by Doppler echocardiography: contribution of duration of pulmonary venous versus mitral flow velocity curves at atrial contraction. J Am Soc Echocardiogr 1997;10:52-9.

59. Abu-Yousef MM. Normal and respiratory variations of the hepatic and portal venous duplex Doppler waveforms with simultaneous electrocardiographic correlation. J Ultrasound Med 1992;11:263-8.

60. Hsia TY, Khambadkone S, Redington AN, Migliavacca F, Deanfield JE, de Leval MR. Effects of respiration and gravity on infradiaphragmatic venous flow in normal and Fontan patients. Circulation 2000;102: III148-53.

61. Giglia TM, Jenkins KJ, Matitiau A, Mandell VS, Sanders SP, Mayer JE Jr., et al. Influence of right heart size on outcome in pulmonary atresia with intact ventricular septum. Circulation 1993;88:2248-56.

62. Hanley FL, Sade RM, Blackstone EH, Kirklin JW, Freedom RM, Nanda NC. Outcomes in neonatal pulmonary atresia with intact ventricular septum. A multiinstitutional study. J Thorac Cardiovasc Surg 1993; 105:406-27.

63. Bull C, de Leval MR, Mercanti C, Macartney FJ, Anderson RH. Pulmonary atresia and intact ventricular septum: a revised classification. Circulation 1982;66:266-72.

64. Rhodes LA, Colan SD, Perry SB, Jonas RA, Sanders SP. Predictors of survival in neonates with critical aortic stenosis. Circulation 1991;84: 2325-35.

65. Gutgesell HP, Bricker JT, Colvin EV, Latson LA, Hawkins EP. Atrioventricular valve annular diameter: two-dimensional echocardiographic-autopsy correlation. Am J Cardiol 1984;53:1652-5.

66. King DH, Smith EO, Huhta JC, Gutgesell HP. Mitral and tricuspid valve annular diameter in normal children determined by two-dimensional echocardiography. Am J Cardiol 1985;55:787-9.

67. Tacy TA, Vermilion RP, Ludomirsky A. Range of normal valve annulus size in neonates. Am J Cardiol 1995;75:541-3.

68. Tei C, Pilgrim JP, Shah PM, Ormiston JA, Wong M. The tricuspid valve annulus: study of size and motion in normal subjects and in patients with tricuspid regurgitation. Circulation 1982;66:665-71.

69. Poutanen T, Tikanoja T, Sairanen H, Jokinen E. Normal mitral and aortic valve areas assessed by three- and two-dimensional echocardiography in 168 children and young adults. Pediatr Cardiol 2006;27:217-25.

70. Kaplan SR, Bashein G, Sheehan FH, Legget ME, Munt B, Li XN, et al. Three-dimensional echocardiographic assessment of annular shape changes in the normal and regurgitant mitral valve. Am Heart J 2000; 139:378-87.

71. Riggs TW, Lapin GD, Paul MH, Muster AJ, Berry TE. Measurement of mitral valve orifice area in infants and children by two-dimensional echocardiography. J Am Coll Cardiol 1983;1:873-8.

72. Fyrenius A, Engvall J, Janerot-Sjoberg B. Major and minor axes of the normal mitral annulus. J Heart Valve Dis 2001;10:146-52.

73. Sairanen H, Louhimo I. Dimensions of the heart and great vessels in normal children. A postmortem study of cardiac ventricles, valves and great vessels. Scand J Thorac Cardiovasc Surg 1992;26:83-92.

74. Foster GP, Dunn AK, Abraham S, Ahmadi N, Sarraf G. Accurate measurement of mitral annular dimensions by echocardiography: importance of correctly aligned imaging planes and anatomic landmarks. J Am Soc Echocardiogr 2009;22:458-63.

75. Snider AR, Serwer GA, Ritter SB. Methods for obtaining quantitative information from the echocardiographic examination. In: Echocardiography in pediatric heart disease. St. Louis, MO: Mosby; 1997. 133–234.

76. Baumgartner H, Hung J, Bermejo J, Chambers JB, Evangelista A, Griffin BP, et al. Echocardiographic assessment of valve stenosis: EAE/ASE recommendations for clinical practice. J Am Soc Echocardiogr 2009;22:1-23.

77. Binder TM, Rosenhek R, Porenta G, Maurer G, Baumgartner H. Improved assessment of mitral valve stenosis by volumetric real-time three-dimensional echocardiography. J Am Coll Cardiol 2000;36:1355-61.

78. Bonow RO, Carabello BA, Chatterjee K, de Leon AC Jr., Faxon DP, Freed MD, et al. ACC/AHA 2006 guidelines for the management of patients with valvular heart disease: a report of the American College of Cardiology/American Heart Association Task Force on Practice Guidelines (Writing Committee to Revise the 1998 Guidelines for the Management of Patients With Valvular Heart Disease) developed in collaboration with the Society of Cardiovascular Anesthesiologists endorsed by the Society for Cardiovascular Angiography and Interventions and the Society of Thoracic Surgeons. J Am Coll Cardiol 2006;48:e1-148.

79. Nakatani S, Masuyama T, Kodama K, Kitabatake A, Fujii K, Kamada T. Value and limitations of Doppler echocardiography in the quantification of stenotic mitral valve area: comparison of the pressure half-time and the continuity equation methods. Circulation 1988;77:78-85.

80. Banerjee A, Kohl T, Silverman NH. Echocardiographic evaluation of congenital mitral valve anomalies in children. Am J Cardiol 1995;76: 1284-91.

81. Zoghbi WA, Enriquez-Sarano M, Foster E, Grayburn PA, Kraft CD, Levine RA, et al. Recommendations for evaluation of the severity of native valvular regurgitation with two-dimensional and Doppler echocardiography. J Am Soc Echocardiogr 2003;16:777-802.

82. Donovan CL, Armstrong WF, Bach DS. Quantitative Doppler tissue imaging of the left ventricular myocardium: validation in normal subjects. Am Heart J 1995;130:100-4.

83. Garcia MJ, Rodriguez L, Ares M, Griffin BP, Klein AL, Stewart WJ, et al. Myocardial wall velocity assessment by pulsed Doppler tissue imaging: characteristic findings in normal subjects. Am Heart J 1996; 132:648-56.

84. Pai RG, Gill KS. Amplitudes, durations, and timings of apically directed left ventricular myocardial velocities: II. Systolic and diastolic asynchrony in patients with left ventricular hypertrophy. J Am Soc Echocardiogr 1998;11:112-8.

85. Feigenbaum H, Armstrong WF, Ryan T. Evaluation of systolic and diastolic function of the left ventricle. In: Feigenbaum's echocardiography. Philadelphia: Lippincott Williams & Wilkins; 2005. pp. 138-80.

86. Rokey R, Kuo LC, Zoghbi WA, Limacher MC, Quinones MA. Determination of parameters of left ventricular diastolic filling with pulsed Doppler echocardiography: comparison with cineangiography. Circulation 1985;71:543-50.

87. Bowman LK, Lee FA, Jaffe CC, Mattera J, Wackers FJ, Zaret BL. Peak filling rate normalized to mitral stroke volume: a new Doppler echocardiographic filling index validated by radionuclide angiographic techniques. J Am Coll Cardiol 1988;12:937-43.

88. Nascimento R, Pereira D, Freitas A, Pereira E, Mendonca I, Dinis M. Comparison of left ventricular ejection fraction in congenital heart disease by visual versus algorithmic determination. Am J Cardiol 1997; 80:1331-5.

89. Schwartz ML, Gauvreau K, Geva T. Predictors of outcome of biventricular repair in infants with multiple left heart obstructive lesions. Circulation 2001;104:682-7.

90. Colan SD, McElhinney DB, Crawford EC, Keane JF, Lock JE. Validation and re-evaluation of a discriminant model predicting anatomic suitability for biventricular repair in neonates with aortic stenosis. J Am Coll Cardiol 2006;47:1858-65.

91. Vogel M, Staller W, Buhlmeyer K. Left ventricular myocardial mass determined by cross-sectional echocardiography in normal newborns, infants, and children. Pediatr Cardiol 1991;12:143-9.

92. Regen DM, Graham TP, Wyse RK, Deanfield J, Franklin RC. Left-ventricular cavity dimensions in children with normal and dilated hearts. Pediatr Cardiol 1988;9:17-24.

93. Nosir YF, Vletter WB, Boersma E, Frowijn R, ten Cate FJ, Fioretti PM, et al. The apical long-axis rather than the two-chamber view should be used in combination with the four-chamber view for accurate assessment of left ventricular volumes and function. Eur Heart J 1997;18:1175-85.

94. Malm S, Sagberg E, Larsson H, Skjaerpe T. Choosing apical long-axis instead of two-chamber view gives more accurate biplane echocardiographic measurements of left ventricular ejection fraction: a comparison with magnetic resonance imaging. J Am Soc Echocardiogr 2005;18:1044-50.

95. Wyatt HL, Heng MK, Meerbaum S, Gueret P, Hestenes J, Dula E, et al. Cross-sectional echocardiography. II. Analysis of mathematic models for quantifying volume of the formalin-fixed left ventricle. Circulation 1980;61:1119-25.

96. Mercier JC, DiSessa TG, Jarmakani JM, Nakanishi T, Hiraishi S, Isabel-Jones J, et al. Two-dimensional echocardiographic assessment of left ventricular volumes and ejection fraction in children. Circulation 1982;65: 962-9.

97. Wyatt HL, Meerbaum S, Heng MK, Gueret P, Corday E. Cross-sectional echocardiography. III. Analysis of mathematic models for quantifying volume of symmetric and asymmetric left ventricles. Am Heart J 1980; 100:821-8.

98. Devereux RB, Pini R, Aurigemma GP, Roman MJ. Measurement of left ventricular mass: methodology and expertise. J Hypertens 1997;15: 801-9.

99. Devereux RB. Detection of left ventricular hypertrophy by M-mode echocardiography. Anatomic validation, standardization, and comparison to other methods. Hypertension 1987;9:II19-26.

100. Gottdiener JS, Bednarz J, Devereux R, Gardin J, Klein A, Manning WJ, et al. American Society of Echocardiography recommendations for use of echocardiography in clinical trials. J Am Soc Echocardiogr 2004;17: 1086-119.

101. Hanevold C, Waller J, Daniels S, Portman R, Sorof J. The effects of obesity, gender, and ethnic group on left ventricular hypertrophy and geometry in hypertensive children: a collaborative study of the International Pediatric Hypertension Association. Pediatrics 2004;113:328-33.

102. Daniels SR, Loggie JM, Khoury P, Kimball TR. Left ventricular geometry and severe left ventricular hypertrophy in children and adolescents with essential hypertension. Circulation 1998;97:1907-11.

103. Kimball TR, Daniels SR, Loggie JM, Khoury P, Meyer RA. Relation of left ventricular mass, preload, afterload and contractility in pediatric patients with essential hypertension. J Am Coll Cardiol 1993;21:997-1001.

104. Jenkins C, Bricknell K, Hanekom L, Marwick TH. Reproducibility and accuracy of echocardiographic measurements of left ventricular parameters using real-time three-dimensional echocardiography. J Am Coll Cardiol 2004;44:878-86.

105. Soliman OI, Kirschbaum SW, van Dalen BM, van der Zwaan HB, Delavary BM, Vletter WB, et al. Accuracy and reproducibility of quantitation of left ventricular function by real-time three-dimensional echocardiography versus cardiac magnetic resonance. Am J Cardiol 2008;102: 778-83.

106. van den Bosch AE, Robbers-Visser D, Krenning BJ, McGhie JS, Helbing WA, Meijboom FJ, et al. Comparison of real-time three-dimensional echocardiography to magnetic resonance imaging for assessment of left ventricular mass. Am J Cardiol 2006;97:113-7.

107. Arai K, Hozumi T, Matsumura Y, Sugioka K, Takemoto Y, Yamagishi H, et al. Accuracy of measurement of left ventricular volume and ejection fraction by new real-time three-dimensional echocardiography in patients with wall motion abnormalities secondary to myocardial infarction. Am J Cardiol 2004;94:552-8.

108. Lu X, Xie M, Tomberlin D, Klas B, Nadvoretskiy V, Ayres N, et al. How accurately, reproducibly, and efficiently can we measure left ventricular indices using M-mode, 2-dimensional, and 3-dimensional echocardiography in children? Am Heart J 2008;155:946-53.

109. Riehle TJ, Mahle WT, Parks WJ, Sallee D III, Fyfe DA. Real-time three-dimensional echocardiographic acquisition and quantification of left ventricular indices in children and young adults with congenital heart disease: comparison with magnetic resonance imaging. J Am Soc Echocardiogr 2008;21:78-83.

110. Iino M, Shiraishi H, Ichihashi K, Hoshina M, Saitoh M, Hirakubo Y, et al. Volume measurement of the left ventricle in children using real-time three-dimensional echocardiography: comparison with ventriculography. J Cardiol 2007;49:221-9.

111. Lipshultz SE, Colan SD, Gelber RD, Perez-Atayde AR, Sallan SE, Sanders SP. Late cardiac effects of doxorubicin therapy for acute lymphoblastic leukemia in childhood. N Engl J Med 1991;324:808-15.

112. Lipshultz SE, Orav EJ, Sanders SP, McIntosh K, Colan SD. Limitations of fractional shortening as an index of contractility in pediatric patients infected with human immunodeficiency virus. J Pediatr 1994;125: 563-70.

113. Colan SD, Borow KM, Neumann A. Left ventricular end-systolic wall stress-velocity of fiber shortening relation: a load-independent index of myocardial contractility. J Am Coll Cardiol 1984;4:715-24.

114. Pai RG, Gill KS. Amplitudes, durations, and timings of apically directed left ventricular myocardial velocities: I. Their normal pattern and coupling to ventricular filling and ejection. J Am Soc Echocardiogr 1998;11:105-11.

115. Sohn DW, Chai IH, Lee DJ, Kim HC, Kim HS, Oh BH, et al. Assessment of mitral annulus velocity by Doppler tissue imaging in the evaluation of left ventricular diastolic function. J Am Coll Cardiol 1997;30:474-80.

116. Nikitin NP, Witte KK, Thackray SD, de Silva R, Clark AL, Cleland JG. Longitudinal ventricular function: normal values of atrioventricular annular and myocardial velocities measured with quantitative two-dimensional color Doppler tissue imaging. J Am Soc Echocardiogr 2003;16:906-21.

117. Eidem BW, McMahon CJ, Cohen RR, Wu J, Finkelshteyn I, Kovalchin JP, et al. Impact of cardiac growth on Doppler tissue imaging velocities: a study in healthy children. J Am Soc Echocardiogr 2004;17:212-21.

118. Roberson DA, Cui W, Chen Z, Madronero LF, Cuneo BF. Annular and septal Doppler tissue imaging in children: normal z-score tables and effects of age, heart rate, and body surface area. J Am Soc Echocardiogr 2007;20:1276-84.

119. Kukulski T, Voigt JU, Wilkenshoff UM, Strotmann JM, Wranne B, Hatle L, et al. A comparison of regional myocardial velocity information derived by pulsed and color Doppler techniques: an in vitro and in vivo study. Echocardiography 2000;17:639-51.

120. Van de Veire NR, De Sutter J, Bax JJ, Roelandt JR. Technological advances in tissue Doppler imaging echocardiography. Heart 2008; 94:1065-74.

121. Rudko R, Przewlocki T, Pasowicz M, Biernacka B, Kablak-Ziembicka A, Tracz W. IVRT'/IVRT index is a useful tool for detection of elevated left ventricular filling pressure in patients with preserved ejection fraction. Echocardiography 2008;25:473-81.

122. Vogel M, Schmidt MR, Kristiansen SB, Cheung M, White PA, Sorensen K, et al. Validation of myocardial acceleration during isovolumic contraction as a novel noninvasive index of right ventricular contractility: comparison with ventricular pressure-volume relations in an animal model. Circulation 2002;105:1693-9.

123. Rychik J, Tian ZY. Quantitative assessment of myocardial tissue velocities in normal children with Doppler tissue imaging. Am J Cardiol 1996;77: 1254-7.

124. O'Leary PW, Durongpisitkul K, Cordes TM, Bailey KR, Hagler DJ, Tajik J, et al. Diastolic ventricular function in children: a Doppler echocardiographic study establishing normal values and predictors of increased ventricular end-diastolic pressure. Mayo Clin Proc 1998;73:616-28.

125. Ayabakan C, Ozkutlu S. Left ventricular myocardial velocities in healthy children: quantitative assessment by tissue Doppler echocardiography and relation to the characteristics of filling of the left ventricle. Cardiol Young 2004;14:156-63.

126. Hiarada K, Orino T, Yasuoka K, Tamura M, Takada G. Tissue doppler imaging of left and right ventricles in normal children. Tohoku J Exp Med 2000;191:21-9.

127. Kapusta L, Thijssen JM, Cuypers MH, Peer PG, Daniels O. Assessment of myocardial velocities in healthy children using tissue Doppler imaging. Ultrasound Med Biol 2000;26:229-37.

128. Mori K, Hayabuchi Y, Kuroda Y, Nii M, Manabe T. Left ventricular wall motion velocities in healthy children measured by pulsed wave Doppler tissue echocardiography: normal values and relation to age and heart rate. J Am Soc Echocardiogr 2000;13:1002-11.

129. Frommelt PC, Ballweg JA, Whitstone BN, Frommelt MA. Usefulness of Doppler tissue imaging analysis of tricuspid annular motion for determination of right ventricular function in normal infants and children. Am J Cardiol 2002;89:610-3.

130. Rhodes J, Fulton DR, Levine JC, Marx GR. Comparison between the mean dP/dt during isovolumetric contraction and other echocardiographic indexes of ventricular systolic function. Echocardiography 1997;14:215-22.

131. Rhodes J, Udelson JE, Marx GR, Schmid CH, Konstam MA, Hijazi ZM, et al. A new noninvasive method for the estimation of peak dP/dt. Circulation 1993;88:2693-9.

132. Border WL, Michelfelder EC, Glascock BJ, Witt SA, Spicer RL, Beekman RH III, et al. Color M-mode and Doppler tissue evaluation of diastolic function in children: simultaneous correlation with invasive indices. J Am Soc Echocardiogr 2003;16:988-94.

133. Brun P, Tribouilloy C, Duval AM, Iserin L, Meguira A, Pelle G, et al. Left ventricular flow propagation during early filling is related to wall relaxation: a color M-mode Doppler analysis. J Am Coll Cardiol 1992;20: 420-32.

134. Takatsuji H, Mikami T, Urasawa K, Teranishi J, Onozuka H, Takagi C, et al. A new approach for evaluation of left ventricular diastolic function: spatial and temporal analysis of left ventricular filling flow propagation by color M-mode Doppler echocardiography. J Am Coll Cardiol 1996;27: 365-71.

135. Tei C. New non-invasive index for combined systolic and diastolic ventricular function. J Cardiol 1995;26:135-6.

136. Eidem BW, Tei C, O'Leary PW, Cetta F, Seward JB. Nongeometric quantitative assessment of right and left ventricular function: myocardial performance index in normal children and patients with Ebstein anomaly. J Am Soc Echocardiogr 1998;11:849-56.

137. Friedberg MK, Slorach C. Relation between left ventricular regional radial function and radial wall motion abnormalities using two-dimensional speckle tracking in children with idiopathic dilated cardiomyopathy. Am J Cardiol 2008;102:335-9.

138. Ramani GV, Bazaz R, Edelman K, Lopez-Candales A. Pulmonary hypertension affects left ventricular basal twist: a novel use for speckle-tracking imaging. Echocardiography 2009;26:44-51.

139. Goffinet C, Chenot F, Robert A, Pouleur AC, de Waroux JB, Vancrayenest D, et al. Assessment of subendocardial vs. subepicardial left ventricular rotation and twist using two-dimensional speckle tracking echocardiography: comparison with tagged cardiac magnetic resonance. Eur Heart J 2009;30:608-17.

140. van Dalen BM, Soliman OI, Vletter WB, ten Cate FJ, Geleijnse ML. Age-related changes in the biomechanics of left ventricular twist measured by speckle tracking echocardiography. Am J Physiol Heart Circ Physiol 2008;295:H1705-11.

141. Song J, Li C, Tong C, Yang H, Yang X, Zhang J, et al. Evaluation of left ventricular rotation and twist using speckle tracking imaging in patients with atrial septal defect. J Huazhong Univ Sci Technolog Med Sci 2008;28: 190-3.

142. Helbing WA, Bosch HG, Maliepaard C, Rebergen SA, van der Geest RJ, Hansen B, et al. Comparison of echocardiographic methods with magnetic resonance imaging for assessment of right ventricular function in children. Am J Cardiol 1995;76:589-94.

143. Lai WW, Gauvreau K, Rivera ES, Saleeb S, Powell AJ, Geva T. Accuracy of guideline recommendations for two-dimensional quantification of the right ventricle by echocardiography. Int J Cardiovasc Imaging 2008;24: 691-8.

144. Cooper MJ, Teitel DF, Silverman NH, Enderlein M. Comparison of M-mode echocardiographic measurement of right ventricular wall thickness obtained by the subcostal and parasternal approach in children. Am J Cardiol 1984;54:835-8.

145. Jiang L, Wiegers SE, Weyman AE. Right ventricle. In: Weyman AE, editor. Principles and practice of echocardiography. 2nd ed. Philadelphia: Lea & Febiger; 1994. pp. 901-21.

146. Levine RA, Gibson TC, Aretz T, Gillam LD, Guyer DE, King ME, et al. Echocardiographic measurement of right ventricular volume. Circulation 1984;69:497-505.

147. Silverman NH, Hudson S. Evaluation of right ventricular volume and ejection fraction in children by two-dimensional echocardiography. Pediatr Cardiol 1983;4:197-203.

148. Dell'Italia LJ. The right ventricle: anatomy, physiology, and clinical importance. Curr Probl Cardiol 1991;16:653-720.

149. Haddad F, Hunt SA, Rosenthal DN, Murphy DJ. Right ventricular function in cardiovascular disease, part I: anatomy, physiology, aging, and functional assessment of the right ventricle. Circulation 2008;117: 1436-48.

150. Kaul S, Tei C, Hopkins JM, Shah PM. Assessment of right ventricular function using two-dimensional echocardiography. Am Heart J 1984;107: 526-31.

151. Popescu BA, Antonini-Canterin F, Temporelli PL, Giannuzzi P, Bosimini E, Gentile F, et al. Right ventricular functional recovery after acute myocardial infarction: relation with left ventricular function and interventricular septum motion. GISSI-3 echo substudy. Heart 2005;91:484-8.

152. Koestenberger M, Ravekes W, Everett AD, Stueger HP, Heinzl B, Gamillscheg A, et al. Right ventricular function in infants, children and adolescents: reference values of the tricuspid annular plane systolic excursion (TAPSE) in 640 healthy patients and calculation of z score values. J Am Soc Echocardiogr 2009;22:715-9.

153. Watanabe M, Ono S, Tomomasa T, Okada Y, Kobayashi T, Suzuki T, et al. Measurement of tricuspid annular diastolic velocities by Doppler tissue imaging to assess right ventricular function in patients with congenital heart disease. Pediatr Cardiol 2003;24:463-7.

154. Lytrivi ID, Lai WW, Ko HH, Nielsen JC, Parness IA, Srivastava S. Color Doppler tissue imaging for evaluation of right ventricular systolic function in patients with congenital heart disease. J Am Soc Echocardiogr 2005;18:1099-104.

155. Kutty S, Deatsman SL, Nugent ML, Russell D, Frommelt PC. Assessment of regional right ventricular velocities, strain, and displacement in normal children using velocity vector imaging. Echocardiography 2008;25: 294-307.

156. Samad BA, Alam M, Jensen-Urstad K. Prognostic impact of right ventricular involvement as assessed by tricuspid annular motion in patients with acute myocardial infarction. Am J Cardiol 2002;90:778-81.

157. Kjaergaard J, Snyder EM, Hassager C, Oh JK, Johnson BD. Impact of preload and afterload on global and regional right ventricular function and pressure: a quantitative echocardiography study. J Am Soc Echocardiogr 2006;19:515-21.

158. Lee KS, Abbas AE, Khandheria BK, Lester SJ. Echocardiographic assessment of right heart hemodynamic parameters. J Am Soc Echocardiogr 2007;20:773-82.

159. Nageh MF, Kopelen HA, Zoghbi WA, Quinones MA, Nagueh SF. Estimation of mean right atrial pressure using tissue Doppler imaging. Am J Cardiol 1999;84:1448-51.

160. Sade LE, Gulmez O, Eroglu S, Sezgin A, Muderrisoglu H. Noninvasive estimation of right ventricular filling pressure by ratio of early tricuspid inflow to annular diastolic velocity in patients with and without recent cardiac surgery. J Am Soc Echocardiogr 2007;20:982-8.

161. Moon-Grady AJ, Taylor D, Bennett SH, Hornberger LK, Tacy TA. Color M-mode propagation velocity, but not its ratio to early diastolic inflow velocity, changes throughout gestation in normal human fetuses. Ultrasound Obstet Gynecol 2008;31:535-41.

162. Torbicki A, Skwarski K, Hawrylkiewicz I, Pasierski T, Miskiewicz Z, Zielinski J. Attempts at measuring pulmonary arterial pressure by means of Doppler echocardiography in patients with chronic lung disease. Eur Respir J 1989;2:856-60.

163. Kisanuki A, Tei C, Otsuji Y, Natsugoe K, Kawazoe Y, Arima S, et al. Doppler echocardiographic documentation of diastolic pulmonary artery forward flow. Am J Cardiol 1987;59:711-3.

164. Redington AN, Penny D, Rigby ML, Hayes A. Antegrade diastolic pulmonary arterial flow as a marker of right ventricular restriction after complete repair of pulmonary atresia with intact ventricular septum and critical pulmonary valve stenosis. Cardiol Young 1992;2:382-6.

165. Roberson DA, Cui W. Right ventricular Tei index in children: effect of method, age, body surface area, and heart rate. J Am Soc Echocardiogr 2007;20:764-70.

166. Lindqvist P, Calcutteea A, Henein M. Echocardiography in the assessment of right heart function. Eur J Echocardiogr 2008;9:225-34.

167. Ichida F, Aubert A, Denef B, Dumoulin M, Van der Hauwaert LG. Cross sectional echocardiographic assessment of great artery diameters in infants and children. Br Heart J 1987;58:627-34.

168. Weinert L, Karp R, Vignon P, Bales A, Lang RM. Feasibility of aortic diameter measurement by multiplane transesophageal echocardiography for preoperative selection and preparation of homograft aortic valves. J Thorac Cardiovasc Surg 1996;112:954-61.

169. Otto CM, Burwash IG, Legget ME, Munt BI, Fujioka M, Healy NL, et al. Prospective study of asymptomatic valvular aortic stenosis. Clinical, echocardiographic, and exercise predictors of outcome. Circulation 1997;95:2262-70.

170. De Bruyne B, Pijls NH, Heyndrickx GR, Hodeige D, Kirkeeide R, Gould KL. Pressure-derived fractional flow reserve to assess serial epicardial stenoses: theoretical basis and animal validation. Circulation 2000; 101:1840-7.

171. Baumgartner H, Stefenelli T, Niederberger J, Schima H, Maurer G. "Overestimation" of catheter gradients by Doppler ultrasound in patients with aortic stenosis: a predictable manifestation of pressure recovery. J Am Coll Cardiol 1999;33:1655-61.

172. Niederberger J, Schima H, Maurer G, Baumgartner H. Importance of pressure recovery for the assessment of aortic stenosis by Doppler ultrasound. Role of aortic size, aortic valve area, and direction of the stenotic jet in vitro. Circulation 1996;94:1934-40.

173. Barker PC, Ensing G, Ludomirsky A, Bradley DJ, Lloyd TR, Rocchini AP. Comparison of simultaneous invasive and noninvasive measurements of pressure gradients in congenital aortic valve stenosis. J Am Soc Echocardiogr 2002;15:1496-502.

174. Villavicencio RE, Forbes TJ, Thomas RL, Humes RA. Pressure recovery in pediatric aortic valve stenosis. Pediatr Cardiol 2003;24:457-62.

175. Otto CM, Pearlman AS, Comess KA, Reamer RP, Janko CL, Huntsman LL. Determination of the stenotic aortic valve area in adults using Doppler echocardiography. J Am Coll Cardiol 1986;7:509-17.

176. Baumgartner H, Hung J, Bermejo J, Chambers JB, Evangelista A, Griffin BP, et al. Echocardiographic assessment of valve stenosis: EAE/ASE recommendations for clinical practice. Eur J Echocardiogr 2009;10:1-25.

177. Beroukhim RS, Roosevelt G, Yetman AT. Comparison of the pattern of aortic dilation in children with the Marfan's syndrome versus children with a bicuspid aortic valve. Am J Cardiol 2006;98:1094-5.

178. Chu WC, Mok GC, Lam WW, Yam MC, Sung RY. Assessment of coronary artery aneurysms in paediatric patients with Kawasaki disease by multidetector row CT angiography: feasibility and comparison with 2D echocardiography. Pediatr Radiol 2006;36:1148-53.

179. English RF, Colan SD, Kanani PM, Ettedgui JA. Growth of the aorta in children with Williams syndrome: does surgery make a difference? Pediatr Cardiol 2003;24:566-8.

180. Gussenhoven WJ, van Leenen BF, Kuis W, de Villeneuve VH, Bom N, van Meurs-van Woezik H. Comparison of internal diameter of great arteries in congenital heart disease. A cross-sectional echocardiographic study. Br Heart J 1983;49:45-50.

181. Rossi-Foulkes R, Roman MJ, Rosen SE, Kramer-Fox R, Ehlers KH, O'Loughlin JE, et al. Phenotypic features and impact of beta blocker or calcium antagonist therapy on aortic lumen size in the Marfan syndrome. Am J Cardiol 1999;83:1364-8.

182. Fogel MA, Donofrio MT, Ramaciotti C, Hubbard AM, Weinberg PM. Magnetic resonance and echocardiographic imaging of pulmonary artery size throughout stages of Fontan reconstruction. Circulation 1994;90: 2927-36.

183. Snider AR, Enderlein MA, Teitel DF, Juster RP. Two-dimensional echocardiographic determination of aortic and pulmonary artery sizes from infancy to adulthood in normal subjects. Am J Cardiol 1984;53: 218-24.

184. Sheil ML, Jenkins O, Sholler GF. Echocardiographic assessment of aortic root dimensions in normal children based on measurement of a new ratio of aortic size independent of growth. Am J Cardiol 1995;75: 711-5.

185. Nistri S, Sorbo MD, Basso C, Thiene G. Bicuspid aortic valve: abnormal aortic elastic properties. J Heart Valve Dis 2002;11:369-74.

186. Nkomo VT, Enriquez-Sarano M, Ammash NM, Melton LJ III, Bailey KR, Desjardins V, et al. Bicuspid aortic valve associated with aortic dilatation: a community-based study. Arterioscler Thromb Vasc Biol 2003;23: 351-6.

187. Fedak PW, de Sa MP, Verma S, Nili N, Kazemian P, Butany J, et al. Vascular matrix remodeling in patients with bicuspid aortic valve malformations: implications for aortic dilatation. J Thorac Cardiovasc Surg 2003; 126:797-806.

188. Williams JC, Barratt-Boyes BG, Lowe JB. Supravalvular aortic stenosis. Circulation 1961;24:1311-8.

189. Kurotobi S, Nagai T, Kawakami N, Sano T. Coronary diameter in normal infants, children and patients with Kawasaki disease. Pediatr Int 2002;44: 1-4.

190. Yasuoka K, Harada K, Tamura M, Takada G. Left anterior descending coronary artery flow and its relation to age in children. J Am Soc Echocardiogr 2002;15:69-75.

191. Ordovas KG, Tan C, Reddy GP, Weber OM, Lu Y, Higgins CB. Disparity between ratios of diameters and blood flows in central pulmonary arteries in postoperative congenital heart disease using MRI. J Magn Reson Imaging 2007;25:721-6.

192. Meijboom LJ, Groenink M, van der Wall EE, Romkes H, Stoker J, Mulder BJ. Aortic root asymmetry in Marfan patients; evaluation by magnetic resonance imaging and comparison with standard echocardiography. Int J Card Imaging 2000;16:161-8.